
EQUIMEM: Calibrating Shared Memory in Multi-Agent Debate via Game-Theoretic Equilibrium

Yuqiao Meng¹ Sakshi Sunil Narvekar¹ Luoxi Tang¹ Rupali Rajendra Vaje¹
 Yingxue Zhang¹ Muchao Ye² Zhaohan Xi¹

¹Binghamton University, State University of New York, Binghamton, NY, USA

²University of Iowa, Iowa City, IA, USA

Corresponding to: Zhaohan Xi <zxi@binghamton.edu>

Abstract

Multi-agent debate (MAD) systems increasingly rely on shared memory to support long-horizon reasoning, but this convenience opens a critical vulnerability: a single corrupted entry can contaminate the downstream memory-augmented reasoning, and debate alone fails to filter such errors. Existing safeguards filter entries via heuristics or LLM-based validation, yet they rely on AI judgments that share the same failure modes and overlook the cross-agent dynamics of MAD. We address this gap by formulating memory updating in MAD as a **zero-trust memory game**, in which no agent is assumed honest and the game’s equilibrium serves as an indicator of optimal memory trust. Guided by this equilibrium, we propose EQUIMEM, an inference-time calibration mechanism that quantifies each update algorithmically against the shared memory state, using agents’ existing retrieval queries and traversal paths as evidence rather than soliciting any LLM judgment. EQUIMEM instantiates calibration for both embedding- and graph-based memory, and across diverse benchmarks, MAD frameworks, and memory architectures, it consistently outperforms existing safeguards, remains robust under adversarial agents, and incurs negligible inference overhead.

1 Introduction

Multi-agent debate (MAD) systems built on large language models (LLMs) have shown strong performance on complex reasoning [17, 35, 42, 70], embodied action [57, 71], and planning [24, 33, 38] tasks, where agents iteratively discuss, critique, and refine each other’s outputs [9, 36, 43]. To support interactions beyond a single round, recent MAD systems add a *shared memory* that persists intermediate reasoning, past actions, and episodic trajectories across rounds [3, 69, 89, 94].

While shared memory boosts long-horizon reasoning, it also opens a critical vulnerability: a corrupted memory state, which can subsequently contaminate all downstream memory-augmented reasoning [66]. The corruption arises because individual agents are inherently imperfect: LLMs hallucinate, agree sycophantically [6, 7, 55], or confidently assert incorrect claims [56, 86, 89]. These failures do not cancel under debate. Across recent works, three failure patterns present (Figure 1): (i) an over-confident contributor pushes a hallucinated entry past hedged auditors who defer to its confidence rather than challenge it [17, 72, 82], producing a corrupted memory that reads like established fact; (ii) over-confident auditors veto a tentative but correct contribution [14, 93], producing an over-curated memory that drops truly useful facts; (iii) all agents hedge (or over-confident) and nothing certain is committed [59, 62, 65], leaving memory under-populated. In all three cases, the commit decision depends on agents’ self-reported confidence rather than on any check against the memory state itself, so debate alone cannot filter the errors.

Existing safeguards either filter proposed entries via heuristics or auxiliary LLM classifiers [1, 76], or rely on consensus-based validation [78]. Both deliver real protection, but still produce calibration through AI models that carry the same risks of hallucination and sycophancy. More importantly, these methods are designed for a single agent reading its own memory, and do not model multiple agents continuously writing to (and potentially colluding over) a shared memory space. This gap motivates a critical question: *how can we calibrate memory updates in a MAD system without relying on any single agent’s judgment?*

Answering this question requires re-thinking the cross-agent dynamics of debate itself. Since MAD agents already inspect and critique each other’s contributions, we formulate their interaction with memory as a **zero-trust memory game**. In this formulation, the agent proposing an update acts as a *contributor* in each debating round, while the remaining agents serve as *auditors* who provide evidence about the update’s consistency with current memory. Crucially, no agent is assumed honest in our formulation. We define

game-theoretical utility functions for both roles and show that the game admits an equilibrium whose payoff structure indicates optimal trust in memory: at equilibrium, a contributor cannot raise an update’s influence without also raising its detectability, and an auditor cannot reduce its effort without weakening the consistency signal it produces, which together address the failures as illustrated in Figure 1 (detailed justification is shown in Appendix A.3).

Guided by this equilibrium, we propose EQUIMEM, an equilibrium-guided, inference-time calibration mechanism that requires no LLM call for calibration itself. Agents serve only as signal providers: their existing retrieval queries and traversal paths are intercepted and quantified algorithmically against the full memory state. EQUIMEM instantiates calibration for two representative memory families. For embedding-based memory [69, 94], it checks whether a proposed update disturbs the embedding distribution and reorders retrieval results on auditor queries. For graph-based memory [3, 89], it checks whether new edges are consistent with the local relational neighborhood and with existing multi-hop reasoning paths. In both cases, entries are admitted with trust-discounted weights, so low-confidence content remains available but exerts less influence on downstream retrieval.

We evaluate EQUIMEM on reasoning- and action-intensive benchmarks [39, 57, 87, 88] across three MAD frameworks [37, 49, 79] and four memory architectures [3, 69, 89, 94]. Three findings emerge. (i) *State-aware calibration beats isolated checks*: EQUIMEM ranks first on every benchmark-framework-memory configuration, confirming that errors missed by per-entry scoring are caught only when updates are evaluated against the global memory state. (ii) *Robustness without trust*: even with up to 50% adversarial agents, EQUIMEM stays close to its benign performance, showing that integrity comes from the structural calibration indicator rather than from trusting any individual agent. (iii) *Quality without inflated cost*: since calibration is LLM-free and reuses agents’ existing retrieval activity, EQUIMEM adds zero token overhead and under 5% latency, showing that strong memory protection is achievable without inflating the inference budget.

In summary, this paper makes the following contributions: **(1)** We formulate shared-memory multi-agent debate as a zero-trust memory game, in which the equilibrium payoff structure serves as an indicator of optimal memory trust. **(2)** Guided by this formulation, we propose EQUIMEM, a principled mechanism that calibrates memory updates against the global memory state without trusting any individual agent. **(3)** Through extensive evaluations, EQUIMEM delivers consistent gains over existing baselines, retains effectiveness under adversarial agents, and incurs negligible inference overhead. Code is released at: <https://anonymous.4open.science/r/EquiMem-FE6C>.

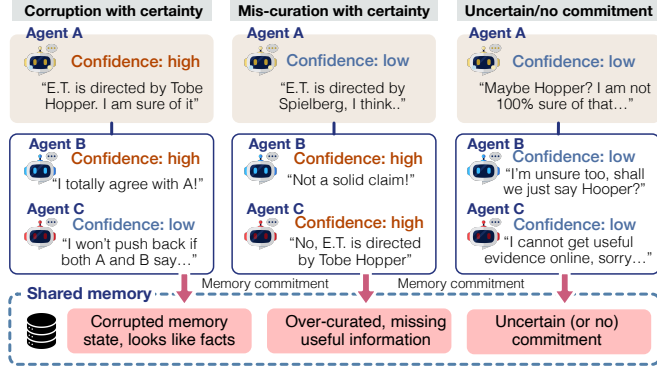


Figure 1: Failures of debate-driven memory commitment.

2 Related Work

Multi-agent debate systems. Multi-agent debate (MAD) improves factuality and reasoning in LLM systems through iterative deliberation among multiple agents [9, 17, 36, 72, 82]. Structural variants include role-conditioned debate [9, 77], dynamic participant selection [10, 37], and tournament-style aggregation [28, 95]. Theoretical work studies the consensus properties of debate [58, 91] and its vulnerability to adversarial participants [2, 34]. To enable cross-task learning, recent systems pair debate with a shared memory that persists across rounds [23, 49, 89].

Memory design for LLM agents. Agent memory has evolved from fixed context windows to structured persistent stores [45, 46, 94]. Common designs include embedding-based retrieval [56, 69, 94], graph-structured memory [12, 51], and hierarchical or multi-tier storage [45, 75, 84]. These systems are typically optimised for retrieval quality, with veracity and provenance treated as secondary [61, 80, 92]. Multi-agent variants extend the same designs to a shared store accessible to several agents at once [49, 52, 89].

LLM hallucinations and memory safety. LLMs frequently produce plausible-sounding but incorrect content [5, 25, 26, 85]. Common mitigations include retrieval augmentation [19, 32], self-consistency verification [41, 60], and uncertainty calibration [27, 53, 64, 83]. Beyond intrinsic errors, conflicts between retrieved memories further complicate downstream reasoning [68, 74]. A growing body of work targets memory specifically: AgentPoison injects backdoors into memory banks [11], MINJA achieves memory corruption through query-only interaction [15, 16], and related studies expose vulnerabilities across multi-agent communication channels [2, 31, 90]. On the defence side, perplexity-based filters [1] and LLM-based auditors [81] score individual entries before commit, while A-MemGuard [78] validates entries through consensus over reasoning paths derived from related memories.

3 Problem Formulation: Zero-Trust Memory Game

This section formalizes memory-based multi-agent debate as a **zero-trust memory game**, where no agent’s contribution to memory \mathcal{M} is assumed honest. Agents iterate between two roles: a *contributor* who writes reasoning traces with factual claims into \mathcal{M} , and *auditors* who inspect those contributions for hallucinations or adversarial content. Our goal is to design a set of game-theoretic rules, namely, the **utility functions** for contributor and auditors, respectively, to remove the need to trust any individual agent and achieve honest memory behavior on the whole-system.

3.1 Setup and Notation for Shared-Memory Multi-Agent Debate

We consider a shared-memory multi-agent debate system $\mathcal{G} = (\mathcal{N}, \mathcal{M})$ where $\mathcal{N} = \{a_1, \dots, a_n\}$ is a set of n agents operating over a shared memory \mathcal{M} . We denote \mathcal{M}_t as a memory state at each debate round t . Besides agents’ original roles, we assign two real-time roles at each round t : The agent that proposes new reasoning, facts, or beliefs is referred to as the **contributor**, denoted by $a_c \in \mathcal{N}$, who generates a proposal Δ_t to be written into \mathcal{M}_t . The remaining agents $\mathcal{A}_t = \mathcal{N} \setminus \{a_c\}$ form the **auditors**, tasked with evaluating whether Δ_t should be committed. A successful commit transitions the memory state as: $\mathcal{M}_{t+1} = \text{Merge}(\mathcal{M}_t, \Delta_t)$ with an architecture-specific memory integration function $\text{Merge}(\cdot, \cdot)$ and the raw memory space \mathbb{D} for all possible Δ_t .

3.2 The Zero-Trust Memory Game

Rationale. Recent work has shown that LLM-based agents are susceptible to sycophantic agreement [18, 55], misrepresentation [48], and belief perseveration [50], all undermining the reliability of agents acting as honest contributors or auditors. Classical fault-tolerance models (e.g., Byzantine fault tolerance [8, 30]) address a bounded fraction of faulty agents but assume the remainder are honest, which is untenable in dynamic agent debating. We therefore adopt a *zero-trust* formulation: no agent is assumed to act in alignment with collective memory integrity, and the system must enforce correctness structurally rather than by trusting any participant. See App. A.1 for a full discussion.

Definition 3.1 (Zero-Trust). *No agent in \mathcal{N} is assumed to act in alignment with memory integrity. Specifically: (i) **The contributor** a_c may craft Δ_t to advance a private objective u_c misaligned with*

the true information state. (ii) **Each auditor** $a_i \in \mathcal{A}_t$ may act to advance its own private objective u_i , which may include collusion with a_c , or adversarial rejection of truthful updates.

This assumption **does not** require that all agents are adversarial, only that none can be *a priori* trusted.

Game Formulation. We formalize memory updating as a two-stage game: In the **contribution stage**, the contributor a_c observes the current memory state \mathcal{M}_t and a private signal $\sigma_c \in \Sigma$ (representing its local reasoning context), and selects a delta:

$$\Delta_t \in \arg \max_{\Delta \in \mathbb{D}} u_c(\Delta, \mathcal{M}_t, \sigma_c) \quad (1)$$

The private utility u_c may encode objectives such as promoting a particular conclusion, inflating confidence estimates, or injecting subtly biased representations into \mathcal{M} .

In the **auditing stage**, each auditor $a_i \in \mathcal{A}_t$ observes Δ_t and the current memory \mathcal{M}_t , and independently emits a binary signal:

$$v_i \in \{0, 1\}, \quad v_i = \pi_i(\Delta_t, \mathcal{M}_t, \sigma_i) \quad (2)$$

where $\sigma_i \in \Sigma$ is a_i 's private signal and π_i is its (potentially mixed) strategy. The aggregate audit decision is formed by a **commitment rule** $\mathcal{C} : \{0, 1\}^{|\mathcal{A}_t|} \rightarrow \{0, 1\}$, such as a weighted majority vote. The update is committed if and only if $\mathcal{C}(\{v_i\}_{i \in \mathcal{A}_t}) = 1$.

3.3 Game-Theoretical Utility Functions and System-Level Equilibrium

Each participant in the game defines a **utility function** to quantify their payoffs in the memory game. At the system level, we leverage an equilibrium of these payoffs to achieve optimal trust in memory.

Contributor utility. The contributor a_c trades off the persuasiveness of Δ_t (the probability it is committed) against the risk of detection:

$$u_c(\Delta_t, \mathcal{M}_t) = \underbrace{\Pr[\mathcal{C}(\{v_i\}) = 1 \mid \Delta_t]}_{\text{commitment gain}} \cdot \underbrace{\mathbb{I}(\Delta_t, \mathcal{M}_t)}_{\text{influence}} - \underbrace{D(\Delta_t, \mathcal{M}_t)}_{\text{detection penalty}} \quad (3)$$

where $\Pr[\mathcal{C}(\{v_i\}) = 1 \mid \Delta_t]$ is the probability of successfully committing Δ_t , $\mathbb{I}(\Delta_t, \mathcal{M}_t)$ measures the downstream influence of Δ_t on future retrievals and reasoning steps, and $D(\Delta_t, \mathcal{M}_t) \in [0, 1]$ is the detectability of Δ_t as inconsistent with \mathcal{M}_t .

Auditor utility. Each auditor a_i evaluates the *alignment* of the proposed Δ_t with the current memory state \mathcal{M}_t :

$$u_i(v_i, \Delta_t, \mathcal{M}_t) = \underbrace{\text{Align}(\Delta_t, \mathcal{M}_t)}_{\text{consistency measure}} - \underbrace{c_i \cdot \mathbf{1}[v_i = \text{scrutinize}]}_{\text{effort cost}} \quad (4)$$

where $\text{Align}(\Delta_t, \mathcal{M}_t) \in [-1, +1]$ measures the semantic and logical consistency of Δ_t with existing memory, which is positive when Δ_t corroborates or extends \mathcal{M}_t , negative when it contradicts or destabilizes it. The $c_i > 0$ is the cost of careful scrutiny. The alignment signal $\text{Align}(\cdot)$ is not self-reported by a_i but is computed by the calibration mechanism Φ from a_i 's submitted evidence (probe queries or attestation paths), ensuring no auditor can manipulate their own utility measurement. The effort cost c_i is estimated online as the empirical computational overhead of a_i 's scrutiny actions across rounds, requiring no pre-specification (see App. A.2).

System-level equilibrium as the indicator of optimal trust in memory. With both utility functions defined above, the system reaches an equilibrium when no participant can improve their payoff by unilaterally changing their strategy: the contributor cannot craft a more influential Δ_t without increasing its detection risk, and no auditor can reduce their scrutiny effort without degrading the alignment signal they produce. Formally:

$$\pi_i^* \in \arg \max_{\pi_i} u_i(\pi_i, \Delta_t^*, \mathcal{M}_t) \quad \forall a_i \in \mathcal{A}_t \quad \text{and} \quad \Delta_t^* \in \arg \max_{\Delta \in \mathbb{D}} u_c(\Delta, \mathcal{M}_t) \quad (5)$$

However, not all equilibria are desirable. Under multi-agent debating, three integrity-degrading equilibria generically emerge: auditors *free-ride* by approving without scrutiny to avoid effort cost c_i ; *colluding* auditors approve Δ_t unconditionally for side benefits; or *adversarial* auditors reject all updates regardless of their quality (Propositions A.1–A.3, App. A.3). These failures echo to incorrect

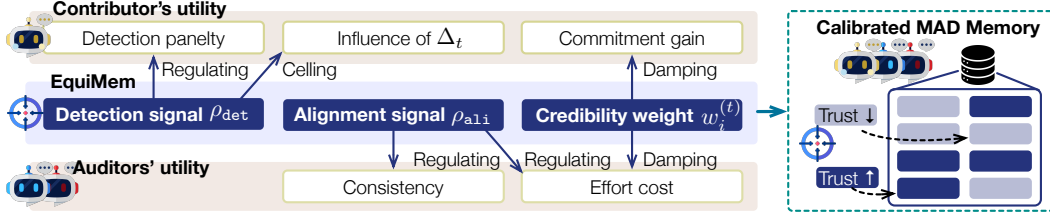


Figure 2: Overview of how the three calibration quantities in EQUIMEM control utility components. See App. C.1 for component-by-component justifications.

memory commitment (Figure 1, detailed in App. A.3) and share a common cause: the commitment outcome depends on auditor votes, giving agents wrong incentives.

To avoid those failure modes, we develop calibration mechanism Φ to break such dependency, i.e., commitment is determined structurally by a calibration indicator ρ , not by votes, which calibrate the memory system without requiring any agent to be honest. Guided by a unified design rationale, we adapt Φ based on specific memory architecture (embedding-based or graph-based) in §4. Due to space constraints, we defer the theoretical guarantees on equilibrium existence, as well as how calibration leads to optimal trust in memory, to App. B.

4 EQUIMEM: Equilibrium-Guided Memory Calibration

4.1 Design Rationale

§3 showed that when the commit decision depends on agent decisions, each agent can improve its own utility and cause incorrect commitment (failures of the equilibrium). Hence, reaching the equilibrium requires that the memory commit decision depend on indicators that no agent can dominate alone. Note that, the equilibrium between u_c and u_i supplies those indicators: The contributor’s u_c (Eq. 3) rewards *influence* over future retrieval, and the auditor’s u_i (Eq. 4) rewards *alignment* with its own reasoning context. A truly informative Δ_t raises both simultaneously. A manipulative Δ_t raises u_c but lowers u_i for any auditor outside the manipulated region. Quantifying Δ_t against this gap reaches the equilibrium without trusting any single agent.

We hence implement the design above as **EQUIMEM**, an inference-time framework that turns each agent’s normal action into evidence. EQUIMEM does not replace agents, as contributors still propose updates and auditors still issue queries or walk paths during debate. Instead, the contributor’s Δ_t is checked against the geometry or topology of \mathcal{M}_t . Each auditor’s existing query or path traversal (used during debate anyway) becomes a **probe** that EQUIMEM samples and quantifies. EQUIMEM never reads agent-reported scores or votes, which turns the three failure modes into actions that either gain nothing or hurt the agent who tries them: an auditor who hides its probe loses credibility weight, an auditor who tries to craft a favorable probe cannot do so because the sample is drawn at random, and an auditor who rejects everything has no rejection power because votes are not used.

Given Δ_t , EQUIMEM produces a calibration indicator $\rho(\Delta_t, \mathcal{M}_t) \in [0, 1]$ that combines (i) a **detection signal** on the contributor side, (ii) an **alignment signal** from auditor probes, and (iii) a **credibility weight** $w_i^{(t)}$ on each auditor’s contribution. Commitment proceeds iff $\rho \geq \rho^*$, where ρ^* is the running median of recent committed scores (cold-start in App. C.2). Committed entries are stored with trust weights proportional to ρ (§4.3). No entry is deleted, so a low-trust entry can be promoted later if new evidence raises its score. Figure 2 shows how EQUIMEM controls game-theoretical utilities (u_c and u_i) with detailed justification in C.1. Noticeably, EQUIMEM incurs marginal latency comparing to base memory-augmented reasoning (App. C.4).

4.2 Architecture-Specific Calibration

We instantiate EQUIMEM on two memory types: embedding-based [69, 94] and graph-based [3, 89]. Episodic and trajectory memories reduce to one of these two for retrieval purposes [3, 69].

Embedding-based memory stores entries as dense vectors $\mathcal{M}_t = \{(\mathbf{e}_j, m_j)\}_{j=1}^N$ with $\mathbf{e}_j = f_\theta(m_j) \in \mathbb{R}^d$. A delta $\Delta_t = \{(\mathbf{e}_k^\Delta, m_k^\Delta)\}_{k=1}^K$ is calibrated in two parallel passes.

The *first pass* computes the detection signal from the local density of each new vector. For each \mathbf{e}_k^Δ we count its dense neighbors and compare to the running average: $\rho_{\text{detect}}(\Delta_t) = 1 - \frac{1}{K} \sum_{k=1}^K \frac{\hat{r}_k}{\bar{r} + \epsilon}$ where \hat{r}_k counts neighbors of \mathbf{e}_k^Δ within an adaptive radius (running median of pairwise similarities in \mathcal{M}_t , App. C.2), and \bar{r} is the running mean neighborhood size. A high \hat{r}_k means the new entry would dominate retrieval across an unusually wide region of memory, which is the high-influence manipulation that u_c rewards.

The *second pass* computes the alignment signal from auditor probes. Each auditor a_i already keeps a queue of pending retrieval queries Q_i during debate. EQUIMEM samples one query $q_i \sim Q_i$ uniformly at random per auditor, so the auditor cannot choose which one is used. We then compute:

$$\rho_{\text{align}}(\Delta_t) = 1 - \frac{1}{|\mathcal{A}_t|} \sum_{i \in \mathcal{A}_t} w_i^{(t)} \cdot d_{\text{RBO}}(\text{top-}k(\mathcal{M}_t, q_i), \text{top-}k(\mathcal{M}_t \cup \Delta_t, q_i)) \quad (6)$$

where $d_{\text{RBO}}(L_1, L_2) \in [0, 1]$ is the rank-biased overlap distance between two lists [13], equal to zero when the lists agree and one when they are disjoint. An informative Δ_t shifts retrieval results across auditors, while a manipulated Δ_t rewrites the top- k auditor-retrieved entries from its original region. The latter produces high d_{RBO} values that push ρ_{align} down.

The credibility weight $w_i^{(t)}$ adds an inter-round cost to cheating. After each round, EQUIMEM checks whether a_i 's probe q_i is *well-formed*: non-empty, syntactically valid, and drawn from the context window the auditor declared. A bad probe pulls the weight toward 0, and a good probe pulls it back toward 1:

$$w_i^{(t+1)} = \begin{cases} w_i^{(t)} \cdot (1 - \delta_t) & \text{if } q_i \text{ is invalid} \\ w_i^{(t)} + \delta_t \cdot (1 - w_i^{(t)}) & \text{if } q_i \text{ is valid} \end{cases} \quad \delta_t = \text{fraction of invalid probes at round } t \quad (7)$$

Both directions move at the same adaptive rate δ_t , so no parameter is tuned. An auditor who slips once recovers after a few clean rounds. An auditor whose long-run invalid rate is p settles at $w^* = 1 - p$, so credibility tracks long-run honesty (proof in App. C.3).

The two passes combine as $\rho = \sqrt{\rho_{\text{detect}} \cdot \rho_{\text{align}}}$. The geometric mean prevents a delta that fails one pass from being saved by the other. The square root keeps $\rho \in [0, 1]$ on the same scale as each pass and avoids the score-shrinking of a plain product.

Graph-based memory stores knowledge as a directed graph $\mathcal{M}_t = (\mathcal{V}_t, \mathcal{E}_t, \ell)$ with edges $\mathcal{E}_t \subseteq \mathcal{V}_t \times \mathcal{R} \times \mathcal{V}_t$. A delta $\Delta_t = (\mathcal{V}_t^\Delta, \mathcal{E}_t^\Delta)$ is first written into a hidden *staging area* $\mathcal{M}_t^{\text{stage}}$. The delta becomes visible only after calibration. Staging blocks adversarial rejection because no agent can see what to reject, and adds no cost because writes use the standard graph-write path.

The *first pass* computes the detection signal from two topological checks per new edge $e = (u, r, v) \in \mathcal{E}_t^\Delta$: (i) The *local check* asks whether e fits u 's existing neighborhood, using a compatibility set $\mathcal{R}_{\text{compat}}(r)$ of relation types that frequently co-occur with r elsewhere in the graph (App. C.6):

$$s_{\text{local}}(e) = \frac{|\{(u, r', v') \in \mathcal{E}_t : r' \in \mathcal{R}_{\text{compat}}(r)\}|}{|\mathcal{N}(u)| + \epsilon} \quad (8)$$

(ii) The *path check* asks whether existing multi-hop paths $\mathcal{P}_{u,v}$ between u and v already support a relation of type r . We enumerate paths $\pi \in \mathcal{P}_{u,v}$ by bidirectional BFS up to depth $L_{\text{max}} = \lceil \log |\mathcal{V}_t| \rceil$, which matches the typical diameter of knowledge graphs and keeps BFS efficient (App. C.7):

$$s_{\text{path}}(e) = \frac{1}{|\mathcal{P}_{uv}|} \sum_{\pi \in \mathcal{P}_{uv}} \mathbf{1}[\text{comp}(r, \text{type}(\pi)) \geq \eta_t] \quad (9)$$

where η_t is the running median of past compatibility scores. Combining the two gives the per-edge score $\rho_{\text{detect}}(e) = \alpha_t s_{\text{local}}(e) + (1 - \alpha_t) s_{\text{path}}(e)$. The weight α_t is the fraction of this round's edges that have at least one supporting path, so it shifts toward whichever check has more evidence. An edge that fails either check raises the detection cost that u_c must pay for manipulation.

The *second pass* computes the alignment signal from auditor probes. Each auditor a_i is already walking some path π_i in \mathcal{M}_t during reasoning. EQUIMEM samples one new edge $e_i^* \in \mathcal{E}_t^\Delta$ uniformly at random per auditor: $\rho_{\text{align}}(\Delta_t) = \frac{1}{|\mathcal{A}_t|} \sum_{i \in \mathcal{A}_t} w_i^{(t)} \cdot \mathbf{1}[\text{reachable}(e_i^*, \pi_i; \mathcal{R}_{\text{compat}})]$, where $\text{reachable}(\cdot)$ is an $O(\log |\mathcal{V}_t|)$ lookup that returns 1 when e_i^* connects to either endpoint of π_i via compatible relations. As in the embedding case, an informative Δ_t extends paths the auditor is already walking, while a manipulative Δ_t adds edges disconnected from existing reasoning. Reachability is a graph-structural fact rather than a semantic judgment, so a failed probe triggers the same credibility decay as Eq. 7.

The two passes combine as $\rho = \sqrt{\rho_{\text{detect}} \cdot \rho_{\text{align}}}$ with $\rho_{\text{detect}} = \frac{1}{|\mathcal{E}_t^\Delta|} \sum_{e \in \mathcal{E}_t^\Delta} \rho_{\text{detect}}(e)$, by the same rationale as the embedding case.

4.3 Memory Retrieval

Calibration shapes both *what gets written* and *how much written entries count when read back*. Each committed entry carries its score ρ as a trust weight. For embedding memory, retrieval re-scales each candidate vector as $\hat{\mathbf{e}}_k = \sqrt{\rho_k} \cdot \mathbf{e}_k$, so low-trust entries sit closer to the origin and are less likely to land in the top- k . For graph memory, a path’s strength is the product $\prod_{e \in \pi} \rho_e$ of trust weights along its edges, so a path through any low-trust edge is automatically discounted. Retrieval cost is unchanged in both cases because trust weights are baked into the index at load time, not computed at query time (App. C.8).

This dual enforcement closes two gaps. A delta that barely passes ρ^* at write time still has a small trust weight, so a contributor cannot inject low-quality content by aiming at the threshold. And when later evidence raises or lowers an entry’s ρ , we update the weight in place rather than delete the entry, so memory remains recoverable as evidence accumulates.

5 Experiments

We evaluate EQUIMEM along three research questions: **RQ1:** How effectively does EQUIMEM maintain memory integrity compared to existing approaches? **RQ2:** How robust is EQUIMEM under different attack strategies? **RQ3:** How much computational overhead does EQUIMEM add?

5.1 Experimental Setup

Datasets. We evaluate on four datasets spanning two groups: **(1) reasoning-intensive**, including HotpotQA [87] (multi-hop question answering) and LoCoMo [39] (long-term conversational memory requiring temporal reasoning across distant dialogue sessions); and **(2) action-intensive**, including ALFWorld [57] (embodied household tasks with sequential action chains) and WebShop [88] (web-based product search and purchase). All require agents to update and retrieve the shared memory.

Baselines. We compare four baseline methods that safeguard agentic memory: **(1) Vanilla:** no additional safeguarding mechanism; LLMs are simply prompted to ensure safe memory use; **(2) LLM-Audit** (used in [78]): an auxiliary LLM scores each proposed Δ_t ; **(3) PPL-Filter** [1]: memory entries whose perplexity under a reference LLM exceeds an adaptive threshold are filtered out; and **(4) A-MemGuard** [78]: consensus is validated across the reasoning paths of agents.

Memory architectures. We evaluate on two embedding-based (vector) memories, Voyager [69] and MemoryBank [94], and two graph-based (structural) memory, AriGraph [3] and G-Memory [89]. We additionally report a No Memory (stateless) baseline as a lower bound.

Backbone of MAD systems. To cover various MAD designs, we integrate EQUIMEM, baselines, and memory architectures into three different MAD systems: AutoGen [79] (conversational turn-taking), MacNet [49] (configurable graph topologies), and DyLAN [37] (dynamic LLM-agent network with learned topology selection).

Other configurations. By default, all evaluations use $6 \times$ Qwen3-VL-8B-Instruct [63] as the MAD backbone besides specification. We defer configuration details, other settings, and results to App. D.

Table 1: Performance comparison with baseline memory safeguarding or calibration approaches. We report accuracy for HotpotQA (HQA), F1 for LoCoMo (LCM), success rate for ALFWorld (ALF), and reward for WebShop (WS) (mean \pm std over 5 runs). Note that A-MemGuard [78] applies only to embedding-based memory (-- otherwise). The **best** and **second best** results are highlighted.

Memory	Method	AutoGen [79]				MacNet [49]				DyLAN [37]			
		HQA	LCM	ALF	WS	HQA	LCM	ALF	WS	HQA	LCM	ALF	WS
Stateless	No-memory	27.5 \pm 5.3	20.2 \pm 7.4	62.1 \pm 2.4	21.4 \pm 7.7	28.6 \pm 2.2	19.8 \pm 1.3	47.3 \pm 6.8	23.5 \pm 5.8	28.4 \pm 2.1	21.0 \pm 4.5	53.8 \pm 4.0	24.9 \pm 8.7
Voyager (emb.)	Vanilla	32.3 \pm 7.4	25.8 \pm 6.1	65.0 \pm 3.6	24.3 \pm 6.1	32.6 \pm 2.9	26.3 \pm 7.3	56.4 \pm 7.3	30.7 \pm 2.5	32.6 \pm 4.3	22.1 \pm 3.6	61.9 \pm 9.2	26.8 \pm 8.4
	+ LLM Audit	33.5 \pm 6.1	28.2 \pm 6.8	66.5 \pm 0.6	25.8 \pm 4.9	34.8 \pm 3.5	31.5 \pm 8.2	57.2 \pm 7.8	37.5 \pm 2.8	36.8 \pm 3.7	27.5 \pm 2.8	66.1 \pm 9.6	29.2 \pm 7.8
	+ PPL Filter	34.6 \pm 5.9	34.1 \pm 6.7	64.2 \pm 1.5	35.2 \pm 6.6	40.2 \pm 1.9	35.7 \pm 6.9	60.1 \pm 6.4	37.8 \pm 2.7	33.5 \pm 3.4	29.2 \pm 3.2	64.8 \pm 7.9	35.5 \pm 6.6
	+ A-MemGuard	42.1 \pm 6.3	37.5 \pm 4.7	72.7 \pm 2.4	31.4 \pm 5.5	43.3 \pm 2.7	43.2 \pm 7.2	65.8 \pm 6.5	39.5 \pm 2.5	41.2 \pm 4.2	33.6 \pm 3.4	74.3 \pm 8.6	41.4 \pm 7.7
	+ EQUIMEM	56.4 \pm 6.3	46.4 \pm 5.5	76.5 \pm 0.4	46.6 \pm 5.6	53.6 \pm 2.6	51.2 \pm 4.4	70.4 \pm 5.4	50.3 \pm 1.5	52.4 \pm 2.5	43.2 \pm 2.8	81.6 \pm 8.5	49.4 \pm 5.8
MemBank (emb.)	Vanilla	33.6 \pm 6.2	21.4 \pm 5.7	64.9 \pm 3.5	25.6 \pm 8.8	33.6 \pm 8.2	20.7 \pm 10.2	48.9 \pm 7.3	24.2 \pm 7.3	29.6 \pm 1.2	24.9 \pm 6.7	55.2 \pm 3.0	27.5 \pm 3.4
	+ LLM Audit	39.2 \pm 5.8	29.2 \pm 5.9	68.6 \pm 3.8	31.6 \pm 7.7	41.4 \pm 7.7	22.8 \pm 10.2	60.3 \pm 11.2	31.8 \pm 7.3	36.5 \pm 1.1	30.4 \pm 6.4	59.3 \pm 3.2	29.1 \pm 3.5
	+ PPL Filter	43.7 \pm 5.1	30.6 \pm 5.9	70.9 \pm 3.5	37.6 \pm 9.7	41.8 \pm 8.7	29.4 \pm 10.4	57.2 \pm 7.2	25.6 \pm 8.0	38.6 \pm 1.3	29.1 \pm 6.2	62.8 \pm 3.3	40.6 \pm 3.8
	+ A-MemGuard	41.1 \pm 4.8	34.1 \pm 5.9	74.0 \pm 3.3	39.1 \pm 6.3	44.5 \pm 6.2	32.7 \pm 7.6	58.5 \pm 9.0	39.6 \pm 7.6	42.3 \pm 0.9	37.2 \pm 5.7	67.5 \pm 2.4	37.3 \pm 3.5
	+ EQUIMEM	52.0 \pm 4.9	39.6 \pm 5.1	79.2 \pm 3.3	46.8 \pm 7.1	56.1 \pm 7.8	38.8 \pm 8.4	66.0 \pm 10.9	55.0 \pm 5.9	53.8 \pm 0.7	42.2 \pm 5.7	71.3 \pm 2.2	51.2 \pm 3.2
AriGraph (graph)	Vanilla	49.2 \pm 2.3	42.3 \pm 3.8	69.4 \pm 5.1	28.9 \pm 4.7	37.7 \pm 3.7	39.8 \pm 4.9	58.3 \pm 4.3	37.4 \pm 10.2	34.8 \pm 4.3	35.4 \pm 13.5	64.1 \pm 6.4	34.6 \pm 5.3
	+ LLM Audit	56.8 \pm 2.2	47.6 \pm 3.0	75.2 \pm 4.2	34.2 \pm 4.0	41.5 \pm 3.2	41.5 \pm 5.1	64.8 \pm 4.5	42.6 \pm 10.8	38.4 \pm 4.0	40.1 \pm 12.7	71.1 \pm 6.8	44.5 \pm 4.7
	+ PPL Filter	53.2 \pm 2.4	52.4 \pm 3.9	76.5 \pm 5.2	38.5 \pm 4.6	45.2 \pm 3.3	49.8 \pm 5.3	66.4 \pm 3.7	46.2 \pm 11.4	43.6 \pm 3.4	46.3 \pm 14.2	66.2 \pm 6.0	45.8 \pm 4.8
	+ A-MemGuard	—	—	—	—	—	—	—	—	—	—	—	—
	+ EQUIMEM	63.3 \pm 1.5	65.2 \pm 3.0	80.5 \pm 3.5	44.1 \pm 4.0	53.7 \pm 3.2	62.7 \pm 2.9	73.1 \pm 4.0	52.5 \pm 9.4	54.0 \pm 3.5	57.3 \pm 9.5	73.1 \pm 4.8	52.6 \pm 4.8
G-Memory (graph)	Vanilla	35.7 \pm 9.2	43.2 \pm 4.1	72.1 \pm 3.8	39.7 \pm 6.3	35.6 \pm 7.9	47.6 \pm 1.5	67.1 \pm 12.5	45.1 \pm 4.4	34.7 \pm 7.7	37.4 \pm 2.8	59.1 \pm 13.6	37.8 \pm 7.9
	+ LLM Audit	38.2 \pm 8.7	49.8 \pm 4.5	76.6 \pm 3.1	41.2 \pm 6.1	40.0 \pm 7.9	51.3 \pm 1.4	68.5 \pm 10.4	49.3 \pm 4.9	41.2 \pm 7.9	40.1 \pm 2.7	67.4 \pm 13.3	45.5 \pm 8.2
	+ PPL Filter	44.5 \pm 8.1	53.2 \pm 4.2	78.4 \pm 3.1	48.6 \pm 6.1	43.2 \pm 7.0	56.8 \pm 1.3	72.6 \pm 10.4	54.7 \pm 3.5	44.1 \pm 8.1	48.6 \pm 2.3	71.5 \pm 11.8	47.2 \pm 6.9
	+ A-MemGuard	—	—	—	—	—	—	—	—	—	—	—	—
	+ EQUIMEM	52.5 \pm 7.8	59.1 \pm 2.9	84.4 \pm 3.2	53.9 \pm 5.8	54.5 \pm 6.2	62.1 \pm 1.4	74.2 \pm 8.1	60.1 \pm 2.9	57.9 \pm 7.1	54.6 \pm 2.2	76.3 \pm 9.9	55.6 \pm 5.5

5.2 Overall Effectiveness (RQ1)

Table 1 reports results across all configurations, which yield several insights:

❶ **State-aware calibration beats isolated checks.** Observe that EQUIMEM ranks first in all columns, and its improvement over the strongest baseline is even larger than the gap separating those baselines from each other. We attribute this to a property of growing memory: as \mathcal{M}_t accumulates entries, the dominant errors are those that read fluently in isolation but conflict with the broader memory state, wherein per-entry checks (LLM Audit, PPL Filter) cannot catch such errors, and even A-MemGuard’s local consensus misses global conflicts. EQUIMEM’s two passes break this constraint by quantifying each Δ_t against \mathcal{M}_t as a whole memory space rather than on isolated memory entries.

❷ **Gains scale inversely with baseline strength.** EQUIMEM’s improvement over the next-best safeguard is largest where baselines are weakest (LoCoMo, WebShop) and smallest where they are already strong (ALFWorld + G-Memory). Calibration acts as an amplifier of memory quality rather than a fixed-offset gain: when fewer errors reach the gating step, EQUIMEM has less to filter.

❸ **Architecture-benchmark interactions are amplified, not flattened.** AriGraph outperforms on multi-hop QA and long-context tasks and G-Memory on action tasks; EQUIMEM amplifies both without modification because the calibration is instantiated from each architecture’s own geometry or topology (§4.2). This also explains why EQUIMEM is the only calibration applicable across all memory designs.

❹ **Gains are robust to MAD.** Absolute performance varies substantially across different MAD backbones, yet EQUIMEM’s ranking and inverse-scaling pattern persist. We explain this by highlighting that EQUIMEM operates at the memory layer, upstream of coordination, so calibration quality is decoupled from orchestration quality.

❺ **Further analysis.** Due to space constraints, we defer the (1) ablation studies and discussions to App. D.4, (2) alternative MAD backbones to App. D.5; (3) the effect of debate rounds to App. D.7, (4) how EQUIMEM addresses memory-commitment failures and provide case studies to App.E, (5) failure modes of EQUIMEM itself to App.F.

5.3 Robustness under Adaptive Attacks (RQ2)

We further test whether EQUIMEM guarantees robustness when k out of N MAD agents are adversarial. We evaluate under two adaptive attack schemes targeting opposite sides of the zero-trust game: (i) *Memory Poisoning* injects fabricated entries to fool ρ_{detect} , while (ii) *Audit Collusion* has adversarial auditors coordinate fabricated probes to inflate ρ_{align} (detailed settings and results in App. D.8).

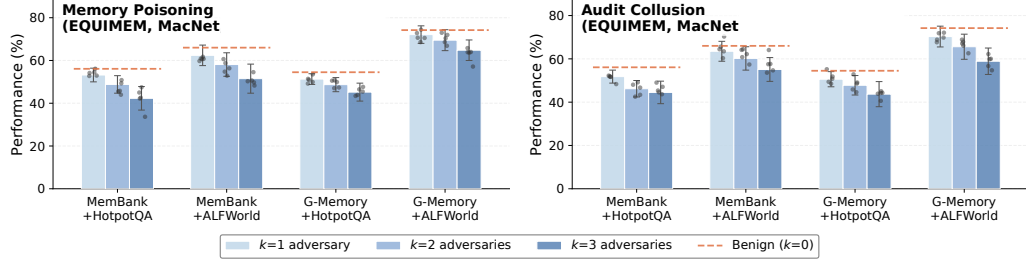


Figure 3: Adversarial robustness of EQUIMEM under two attacks. Bars show performance at $k = 1, 2, 3$ adversarial agents; dashed orange lines show benign performance ($k = 0$). Dots show individual run results (5 seeds). Baseline comparisons are in App. D.8.

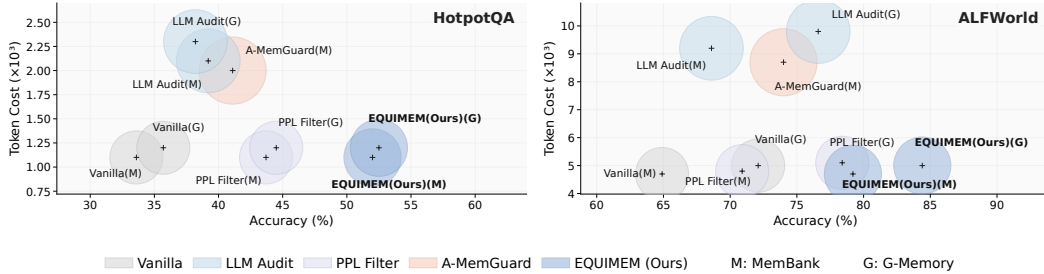


Figure 4: Performance vs. token consumption. Each sub-figure shows MemBank (M) and G-Memory (G) under five calibration methods. Bubble size reflects token-cost variability.

❶ **EQUIMEM degrades gracefully, while baselines collapse dramatically.** Figure 3 shows that EQUIMEM stays within 2-5% of benign performance at $k = 1$ and within 9-16% at $k = 3$. LLM Audit and PPL Filter, as shown in Figure 6, App. D.8, drop by 19-35% at $k = 3$ and frequently fall below the no-memory baseline, i.e., the memory system with its defense becomes worse than no memory at all. The asymmetry traces to a single design choice: EQUIMEM measures Δ_t against the memory space structurally, while baselines score each entry in isolation (or local consensus for A-MemGuard), which is exactly what adversaries exploit by generating fluent, low-perplexity poison.

❷ **Credibility decay is the load-bearing mechanism under attack.** Credibility weighting matters little in benign settings (2-6%, as in Table 8), but under attack it becomes decisive. Adversarial auditors who submit fabricated probes accumulate weight decay over rounds, progressively muting their influence on ρ_{align} . A single adversary’s weight collapses below 0.1 within a few rounds, and even at $k = 3$ the honest majority’s probes still dominate because credibility decays multiplicatively while honest auditors recover toward $w_i \approx 1$. Detailed baseline results are in App. D.8.

5.4 Computational Overhead (RQ3)

A critical property of EQUIMEM is that calibration is LLM-free and algorithmic (§4). Figure 4 measures token consumption, and App. D.9 quantifies inference time latency.

❸ **EQUIMEM matches Vanilla’s token cost while delivering active-defense gains.** EQUIMEM uses the same number of tokens as Vanilla, yet performs far better than every other method (its bubbles sit well to the right). This gain comes at no extra token cost, which is only possible because EQUIMEM’s calibration runs without any LLM call. In contrast, baseline methods pay $\sim 2\times$ tokens for marginal gains: LLM Audit and A-MemGuard nearly double Vanilla’s tokens for only +2 to +9%, since each method requires an LLM call per Δ_t , scaling linearly with the number of deltas and unavoidable without removing the defense.

❹ **EQUIMEM gives the best of both worlds.** No other method achieves both top performance and the lowest cost at the same time. PPL Filter is also free to run but achieves substantially smaller gains than EQUIMEM. This pattern holds across embedding and graph memory and across reasoning and action benchmarks, showing that the LLM-free design is a built-in advantage rather than a lucky

implementation choice. Inference timing (App. D.9) tells the same story: EQUIMEM adds under 5% latency, while LLM-based defenses add 50-94%.

6 Conclusion

This work formulates shared-memory multi-agent debate as a zero-trust memory game and shows that its equilibrium structure indicates optimal trust in memory without assuming any agent honest. Guided by this formulation, we propose EQUIMEM to calibrate memory using agents’ existing retrieval activity as evidence, requiring no LLM call for calibration itself. Across extensive evaluations, EQUIMEM consistently outperforms existing calibration methods, remains robust under up to half adversarial agents, and adds zero token overhead with under marginal latency. These results suggest that strong memory protection in multi-agent systems is achievable without trusting any individual agent or inflating inference cost.

References

- [1] Gabriel Alon and Michael Kamfonas. Detecting language model attacks with perplexity. *arXiv preprint arXiv:2308.14132*, 2023.
- [2] Alfonso Amayuelas, Xianjun Yang, Antonis Antoniadis, Wenyue Hua, Liangming Pan, and William Yang Wang. Multiagent collaboration attack: Investigating adversarial attacks in large language model collaborations via debate. In *Findings of the Association for Computational Linguistics: EMNLP 2024*, pages 6929–6948, 2024.
- [3] Petr Anokhin, Nikita Semenov, Artyom Sorokin, Dmitry Evseev, Andrey Kravchenko, Mikhail Burtsev, and Evgeny Burnaev. Arigraph: Learning knowledge graph world models with episodic memory for llm agents. *arXiv preprint arXiv:2407.04363*, 2024.
- [4] Kenneth J Arrow. *Social choice and individual values*, volume 12. Yale university press, 2012.
- [5] Sourav Banerjee, Ayushi Agarwal, and Saloni Singla. Llms will always hallucinate, and we need to live with this. In *Intelligent Systems Conference*, pages 624–648. Springer, 2025.
- [6] Jaime Banks. Ai sycophancy as social-moral behavior. In *Provoking Generative AI Futures*, pages 99–116. Routledge, 2026.
- [7] María Victoria Carro. Flattering to deceive: The impact of sycophantic behavior on user trust in large language model. *arXiv preprint arXiv:2412.02802*, 2024.
- [8] Miguel Castro, Barbara Liskov, et al. Practical byzantine fault tolerance. In *OsDI*, volume 99, pages 173–186, 1999.
- [9] Chi-Min Chan, Weize Chen, Yusheng Su, Jianxuan Yu, Wei Xue, Shanghang Zhang, Jie Fu, and Zhiyuan Liu. Chateval: Towards better llm-based evaluators through multi-agent debate. *arXiv preprint arXiv:2308.07201*, 2023.
- [10] Weize Chen, Yusheng Su, Jingwei Zuo, Cheng Yang, Chenfei Yuan, Chi-Min Chan, Heyang Yu, Yaxi Lu, Yi-Hsin Hung, Chen Qian, et al. Agentverse: Facilitating multi-agent collaboration and exploring emergent behaviors. In *The Twelfth International Conference on Learning Representations*, 2023.
- [11] Zhaorun Chen, Zhen Xiang, Chaowei Xiao, Dawn Song, and Bo Li. Agentpoison: Red-teaming llm agents via poisoning memory or knowledge bases. *Advances in Neural Information Processing Systems*, 37:130185–130213, 2024.
- [12] Prateek Chhikara, Dev Khant, Saket Aryan, Taranjeet Singh, and Deshraj Yadav. Mem0: Building production-ready ai agents with scalable long-term memory. *arXiv preprint arXiv:2504.19413*, 2025.
- [13] Matteo Corsi and Julián Urbano. The treatment of ties in rank-biased overlap. In *Proceedings of the 47th international ACM SIGIR conference on research and development in information retrieval*, pages 251–260, 2024.

- [14] Justin Cui, Wei-Lin Chiang, Ion Stoica, and Cho-Jui Hsieh. Or-bench: An over-refusal benchmark for large language models. *arXiv preprint arXiv:2405.20947*, 2024.
- [15] Shen Dong, Shaochen Xu, Pengfei He, Yige Li, Jiliang Tang, Tianming Liu, Hui Liu, and Zhen Xiang. Memory injection attacks on llm agents via query-only interaction. *arXiv preprint arXiv:2503.03704*, 2025.
- [16] Shen Dong, Shaochen Xu, Pengfei He, Yige Li, Jiliang Tang, Tianming Liu, Hui Liu, and Zhen Xiang. A practical memory injection attack against llm agents. *arXiv e-prints*, pages arXiv–2503, 2025.
- [17] Yilun Du, Shuang Li, Antonio Torralba, Joshua B Tenenbaum, and Igor Mordatch. Improving factuality and reasoning in language models through multiagent debate. In *Forty-first international conference on machine learning*, 2024.
- [18] Aaron Fanous, Jacob Goldberg, Ank Agarwal, Joanna Lin, Anson Zhou, Sonnet Xu, Vasiliki Bikia, Roxana Daneshjou, and Sanmi Koyejo. Syceval: Evaluating llm sycophancy. In *Proceedings of the AAAI/ACM Conference on AI, Ethics, and Society*, volume 8, pages 893–900, 2025.
- [19] Yunfan Gao, Yun Xiong, Xinyu Gao, Kangxiang Jia, Jinliu Pan, Yuxi Bi, Yixin Dai, Jiawei Sun, Haofen Wang, Haofen Wang, et al. Retrieval-augmented generation for large language models: A survey. *arXiv preprint arXiv:2312.10997*, 2(1):32, 2023.
- [20] John Geanakoplos. Three brief proofs of arrow’s impossibility theorem. *Economic Theory*, 26(1):211–215, 2005.
- [21] Allan Gibbard. Manipulation of voting schemes: a general result. *Econometrica: journal of the Econometric Society*, pages 587–601, 1973.
- [22] Daya Guo, Dejian Yang, Haowei Zhang, Junxiao Song, Peiyi Wang, Qihao Zhu, Runxin Xu, Ruoyu Zhang, Shirong Ma, Xiao Bi, et al. Deepseek-r1: Incentivizing reasoning capability in llms via reinforcement learning. *arXiv preprint arXiv:2501.12948*, 2025.
- [23] Sirui Hong, Mingchen Zhuge, Jonathan Chen, Xiawu Zheng, Yuheng Cheng, Jinlin Wang, Ceyao Zhang, Zili Wang, Steven Ka Shing Yau, Zijuan Lin, et al. Metagpt: Meta programming for a multi-agent collaborative framework. In *The twelfth international conference on learning representations*, 2023.
- [24] Zhe Hu, Hou Pong Chan, Jing Li, and Yu Yin. Debate-to-write: A persona-driven multi-agent framework for diverse argument generation. In *Proceedings of the 31st International Conference on Computational Linguistics*, pages 4689–4703, 2025.
- [25] Lei Huang, Weijiang Yu, Weitao Ma, Weihong Zhong, Zhangyin Feng, Haotian Wang, Qianglong Chen, Weihua Peng, Xiaocheng Feng, Bing Qin, et al. A survey on hallucination in large language models: Principles, taxonomy, challenges, and open questions. *ACM Transactions on Information Systems*, 43(2):1–55, 2025.
- [26] Ziwei Ji, Nayeon Lee, Rita Frieske, Tiezheng Yu, Dan Su, Yan Xu, Etsuko Ishii, Ye Jin Bang, Andrea Madotto, and Pascale Fung. Survey of hallucination in natural language generation. *ACM computing surveys*, 55(12):1–38, 2023.
- [27] Saurav Kadavath, Tom Conerly, Amanda Askell, Tom Henighan, Dawn Drain, Ethan Perez, Nicholas Schiefer, Zac Hatfield-Dodds, Nova DasSarma, Eli Tran-Johnson, et al. Language models (mostly) know what they know. *arXiv preprint arXiv:2207.05221*, 2022.
- [28] Akbir Khan, John Hughes, Dan Valentine, Laura Ruis, Kshitij Sachan, Ansh Radhakrishnan, Edward Grefenstette, Samuel R Bowman, Tim Rocktäschel, and Ethan Perez. Debating with more persuasive llms leads to more truthful answers. *arXiv preprint arXiv:2402.06782*, 2024.
- [29] Harold W Kuhn. Extensive games and the problem of information. *Contributions to the Theory of Games*, 2(28):193–216, 1953.

- [30] Leslie Lamport, Robert Shostak, and Marshall Pease. The byzantine generals problem. In *Concurrency: the works of leslie lamport*, pages 203–226. 2019.
- [31] Donghyun Lee and Mo Tiwari. Prompt infection: Llm-to-llm prompt injection within multi-agent systems. *arXiv preprint arXiv:2410.07283*, 2024.
- [32] Patrick Lewis, Ethan Perez, Aleksandra Piktus, Fabio Petroni, Vladimir Karpukhin, Naman Goyal, Heinrich Küttler, Mike Lewis, Wen-tau Yih, Tim Rocktäschel, et al. Retrieval-augmented generation for knowledge-intensive nlp tasks. *Advances in neural information processing systems*, 33:9459–9474, 2020.
- [33] Han Li, Yuling Shi, Shaoxin Lin, Xiaodong Gu, Heng Lian, Xin Wang, Yantao Jia, Tao Huang, and Qianxiang Wang. Swe-debate: Competitive multi-agent debate for software issue resolution. *arXiv preprint arXiv:2507.23348*, 2025.
- [34] Lin Li, Guikun Chen, Hanrong Shi, Jun Xiao, and Long Chen. A survey on multimodal benchmarks: In the era of large ai models. *arXiv preprint arXiv:2409.18142*, 2024.
- [35] Yunxuan Li, Yibing Du, Jiageng Zhang, Le Hou, Peter Grabowski, Yeqing Li, and Eugene Ie. Improving multi-agent debate with sparse communication topology. In *Findings of the Association for Computational Linguistics: EMNLP 2024*, pages 7281–7294, 2024.
- [36] Tian Liang, Zhiwei He, Wenxiang Jiao, Xing Wang, Yan Wang, Rui Wang, Yujiu Yang, Shuming Shi, and Zhaopeng Tu. Encouraging divergent thinking in large language models through multi-agent debate. In *Proceedings of the 2024 conference on empirical methods in natural language processing*, pages 17889–17904, 2024.
- [37] Zijun Liu, Yanzhe Zhang, Peng Li, Yang Liu, and Diyi Yang. Dynamic llm-agent network: An llm-agent collaboration framework with agent team optimization. *arXiv preprint arXiv:2310.02170*, 2023.
- [38] Chang Ma, Junlei Zhang, Zhihao Zhu, Cheng Yang, Yujiu Yang, Yaohui Jin, Zhenzhong Lan, Lingpeng Kong, and Junxian He. Agentboard: An analytical evaluation board of multi-turn llm agents. *Advances in neural information processing systems*, 37:74325–74362, 2024.
- [39] Adyasha Maharana, Dong-Ho Lee, Sergey Tulyakov, Mohit Bansal, Francesco Barbieri, and Yuwei Fang. Evaluating very long-term conversational memory of llm agents. In *Proceedings of the 62nd Annual Meeting of the Association for Computational Linguistics (Volume 1: Long Papers)*, pages 13851–13870, 2024.
- [40] Yu A Malkov and Dmitry A Yashunin. Efficient and robust approximate nearest neighbor search using hierarchical navigable small world graphs. *IEEE transactions on pattern analysis and machine intelligence*, 42(4):824–836, 2018.
- [41] Potsawee Manakul, Adian Liusie, and Mark Gales. Selfcheckgpt: Zero-resource black-box hallucination detection for generative large language models. In *Proceedings of the 2023 conference on empirical methods in natural language processing*, pages 9004–9017, 2023.
- [42] Yuqiao Meng, Luoxi Tang, Dazheng Zhang, Rafael Brens, Elvys J Romero, Nancy Guo, Safa Elkefi, and Zhaohan Xi. Small agent group is the future of digital health. *arXiv preprint arXiv:2602.08013*, 2026.
- [43] Vrushket More, Lyra Lu, Zeyu Ding, Zhaohan Xi, Seth Mizia, and Nancy L Guo. Theramind: a multi-llm ensemble for accelerating drug repurposing in lung cancer via case report mining. *npj Precision Oncology*, 2026.
- [44] John F Nash Jr. Equilibrium points in n-person games. *Proceedings of the national academy of sciences*, 36(1):48–49, 1950.
- [45] Charles Packer, Vivian Fang, Shishir_G Patil, Kevin Lin, Sarah Wooders, and Joseph_E Gonzalez. Memgpt: towards llms as operating systems. 2023.

- [46] Joon Sung Park, Joseph O’Brien, Carrie Jun Cai, Meredith Ringel Morris, Percy Liang, and Michael S Bernstein. Generative agents: Interactive simulacra of human behavior. In *Proceedings of the 36th annual acm symposium on user interface software and technology*, pages 1–22, 2023.
- [47] David Patterson, Joseph Gonzalez, Urs Hölzle, Quoc Le, Chen Liang, Lluís-Miquel Munguia, Daniel Rothchild, David R So, Maud Texier, and Jeff Dean. The carbon footprint of machine learning training will plateau, then shrink. *Computer*, 55(7):18–28, 2022.
- [48] Ethan Perez, Saffron Huang, Francis Song, Trevor Cai, Roman Ring, John Aslanides, Amelia Glaese, Nat McAleese, and Geoffrey Irving. Red teaming language models with language models. In *Proceedings of the 2022 Conference on Empirical Methods in Natural Language Processing*, pages 3419–3448, 2022.
- [49] Chen Qian, Zihao Xie, Yifei Wang, Wei Liu, Kunlun Zhu, Hanchen Xia, Yufan Dang, Zhuoyun Du, Weize Chen, Cheng Yang, et al. Scaling large language model-based multi-agent collaboration. *arXiv preprint arXiv:2406.07155*, 2024.
- [50] Harsh Raj, Domenic Rosati, and Subhabrata Majumdar. Measuring reliability of large language models through semantic consistency. *arXiv preprint arXiv:2211.05853*, 2022.
- [51] Preston Rasmussen, Pavlo Paliychuk, Travis Beauvais, Jack Ryan, and Daniel Chalef. Zep: a temporal knowledge graph architecture for agent memory. *arXiv preprint arXiv:2501.13956*, 2025.
- [52] Alireza Rezazadeh, Zichao Li, Ange Lou, Yuying Zhao, Wei Wei, and Yujia Bao. Collaborative memory: Multi-user memory sharing in llm agents with dynamic access control. *arXiv preprint arXiv:2505.18279*, 2025.
- [53] Anirban Saha, Binay Gupta, Anirban Chatterjee, and Kunal Banerjee. You believe your llm is not delusional? think again! a study of llm hallucination on foundation models under perturbation. *Discover Data*, 3(1):20, 2025.
- [54] Mark Allen Satterthwaite. Strategy-proofness and arrow’s conditions: Existence and correspondence theorems for voting procedures and social welfare functions. *Journal of economic theory*, 10(2):187–217, 1975.
- [55] Mrinank Sharma, Meg Tong, Tomasz Korbak, David Duvenaud, Amanda Askill, Samuel R Bowman, Newton Cheng, Esin Durmus, Zac Hatfield-Dodds, Scott R Johnston, et al. Towards understanding sycophancy in language models. *arXiv preprint arXiv:2310.13548*, 2023.
- [56] Noah Shinn, Federico Cassano, Ashwin Gopinath, Karthik Narasimhan, and Shunyu Yao. Reflexion: Language agents with verbal reinforcement learning. *Advances in neural information processing systems*, 36:8634–8652, 2023.
- [57] Mohit Shridhar, Xingdi Yuan, Marc-Alexandre Côté, Yonatan Bisk, Adam Trischler, and Matthew Hausknecht. Alfworld: Aligning text and embodied environments for interactive learning. *arXiv preprint arXiv:2010.03768*, 2020.
- [58] Andries Smit, Paul Duckworth, Nathan Grinsztajn, Thomas D Barrett, and Arnu Pretorius. Should we be going mad? a look at multi-agent debate strategies for llms. *arXiv preprint arXiv:2311.17371*, 2023.
- [59] Maojia Song, Tej Deep Pala, Ruiwen Zhou, Weisheng Jin, Amir Zadeh, Chuan Li, Dorien Herremans, and Soujanya Poria. Llms can’t handle peer pressure: Crumbling under multi-agent social interactions. *arXiv preprint arXiv:2508.18321*, 2025.
- [60] Gaurang Sriramanan, Siddhant Bharti, Vinu Sankar Sadasivan, Shoumik Saha, Priyatham Kattakinda, and Soheil Feizi. Llm-check: Investigating detection of hallucinations in large language models. *Advances in Neural Information Processing Systems*, 37:34188–34216, 2024.
- [61] Theodore Sumers, Shunyu Yao, Karthik R Narasimhan, and Thomas L Griffiths. Cognitive architectures for language agents. *Transactions on Machine Learning Research*, 2023.

- [62] Luoxi Tang, Yuqiao Meng, Joseph Costa, Yingxue Zhang, Muchao Ye, and Zhaohan Xi. The value of variance: Mitigating debate collapse in multi-agent systems via uncertainty-driven policy optimization. *arXiv preprint arXiv:2602.07186*, 2026.
- [63] Qwen Team. Qwen3 technical report, 2025.
- [64] Katherine Tian, Eric Mitchell, Allan Zhou, Archit Sharma, Rafael Rafailov, Huaxiu Yao, Chelsea Finn, and Christopher D Manning. Just ask for calibration: Strategies for eliciting calibrated confidence scores from language models fine-tuned with human feedback. In *Proceedings of the 2023 Conference on Empirical Methods in Natural Language Processing*, pages 5433–5442, 2023.
- [65] Christian Tomani, Kamalika Chaudhuri, Ivan Evtimov, Daniel Cremers, and Mark Ibrahim. Uncertainty-based abstention in llms improves safety and reduces hallucinations. *arXiv preprint arXiv:2404.10960*, 2024.
- [66] Vicenç Torra and Maria Bras-Amorós. Memory poisoning and secure multi-agent systems. *arXiv preprint arXiv:2603.20357*, 2026.
- [67] Miles Turpin, Julian Michael, Ethan Perez, and Samuel Bowman. Language models don’t always say what they think: Unfaithful explanations in chain-of-thought prompting. *Advances in Neural Information Processing Systems*, 36:74952–74965, 2023.
- [68] Fei Wang, Xingchen Wan, Ruoxi Sun, Jiefeng Chen, and Sercan O Arik. Astute rag: Overcoming imperfect retrieval augmentation and knowledge conflicts for large language models. In *Proceedings of the 63rd Annual Meeting of the Association for Computational Linguistics (Volume 1: Long Papers)*, pages 30553–30571, 2025.
- [69] Guanzhi Wang, Yuqi Xie, Yunfan Jiang, Ajay Mandlekar, Chaowei Xiao, Yuke Zhu, Linxi Fan, and Anima Anandkumar. Voyager: An open-ended embodied agent with large language models. *arXiv preprint arXiv:2305.16291*, 2023.
- [70] Haotian Wang, Xiyuan Du, Weijiang Yu, Qianglong Chen, Kun Zhu, Zheng Chu, Lian Yan, and Yi Guan. Learning to break: Knowledge-enhanced reasoning in multi-agent debate system. *Neurocomputing*, 618:129063, 2025.
- [71] Junjian Wang, Lidan Zhao, and Xi Sheryl Zhang. Madra: Multi-agent debate for risk-aware embodied planning. *arXiv preprint arXiv:2511.21460*, 2025.
- [72] Qineng Wang, Zihao Wang, Ying Su, Hanghang Tong, and Yangqiu Song. Rethinking the bounds of llm reasoning: Are multi-agent discussions the key? In *Proceedings of the 62nd Annual Meeting of the Association for Computational Linguistics (Volume 1: Long Papers)*, pages 6106–6131, 2024.
- [73] Wenhui Wang, Furu Wei, Li Dong, Hangbo Bao, Nan Yang, and Ming Zhou. Minilm: Deep self-attention distillation for task-agnostic compression of pre-trained transformers. *Advances in neural information processing systems*, 33:5776–5788, 2020.
- [74] Yike Wang, Shangbin Feng, Heng Wang, Weijia Shi, Vidhisha Balachandran, Tianxing He, and Yulia Tsvetkov. Resolving knowledge conflicts in large language models. *arXiv preprint arXiv:2310.00935*, 2023.
- [75] Yu Wang and Xi Chen. Mirix: Multi-agent memory system for llm-based agents. *arXiv preprint arXiv:2507.07957*, 2025.
- [76] Zezhong Wang, Fangkai Yang, Lu Wang, Pu Zhao, Hongru Wang, Liang Chen, Qingwei Lin, and Kam-Fai Wong. Self-guard: Empower the llm to safeguard itself. In *Proceedings of the 2024 Conference of the North American Chapter of the Association for Computational Linguistics: Human Language Technologies (Volume 1: Long Papers)*, pages 1648–1668, 2024.
- [77] Zhenhailong Wang, Shaoguang Mao, Wenshan Wu, Tao Ge, Furu Wei, and Heng Ji. Unleashing the emergent cognitive synergy in large language models: A task-solving agent through multi-persona self-collaboration. In *Proceedings of the 2024 Conference of the North American Chapter of the Association for Computational Linguistics: Human Language Technologies (Volume 1: Long Papers)*, pages 257–279, 2024.

- [78] Qianshan Wei, Tengchao Yang, Yaochen Wang, Xinfeng Li, Lijun Li, Zhenfei Yin, Yi Zhan, Thorsten Holz, Zhiqiang Lin, and XiaoFeng Wang. A-memguard: A proactive defense framework for llm-based agent memory. *arXiv preprint arXiv:2510.02373*, 2025.
- [79] Qingyun Wu, Gagan Bansal, Jieyu Zhang, Yiran Wu, Beibin Li, Erkang Zhu, Li Jiang, Xiaoyun Zhang, Shaokun Zhang, Jiale Liu, et al. Autogen: Enabling next-gen llm applications via multi-agent conversations. In *First conference on language modeling*, 2024.
- [80] Yaxiong Wu, Sheng Liang, Chen Zhang, Yichao Wang, Yongyue Zhang, Huifeng Guo, Ruiming Tang, and Yong Liu. From human memory to ai memory: A survey on memory mechanisms in the era of llms. *arXiv preprint arXiv:2504.15965*, 2025.
- [81] Zhen Xiang, Linzhi Zheng, Yanjie Li, Junyuan Hong, Qinbin Li, Han Xie, Jiawei Zhang, Zidi Xiong, Chulin Xie, Carl Yang, et al. Guardagent: Safeguard llm agents by a guard agent via knowledge-enabled reasoning. *arXiv preprint arXiv:2406.09187*, 2024.
- [82] Kai Xiong, Xiao Ding, Yixin Cao, Ting Liu, and Bing Qin. Examining inter-consistency of large language models collaboration: An in-depth analysis via debate. In *Findings of the Association for Computational Linguistics: EMNLP 2023*, pages 7572–7590, 2023.
- [83] Miao Xiong, Zhiyuan Hu, Xinyang Lu, Yifei Li, Jie Fu, Junxian He, and Bryan Hooi. Can llms express their uncertainty? an empirical evaluation of confidence elicitation in llms. *arXiv preprint arXiv:2306.13063*, 2023.
- [84] Wujiang Xu, Zujie Liang, Kai Mei, Hang Gao, Juntao Tan, and Yongfeng Zhang. A-mem: Agentic memory for llm agents. *arXiv preprint arXiv:2502.12110*, 2025.
- [85] Ziwei Xu, Sanjay Jain, and Mohan Kankanhalli. Hallucination is inevitable: An innate limitation of large language models. *arXiv preprint arXiv:2401.11817*, 2024.
- [86] Shuai Yang, Qi Yang, Luoxi Tang, Yuqiao Meng, Nancy Guo, Jeremy Blackburn, and Zhaohan Xi. On the eligibility of llms for counterfactual reasoning: a decompositional study. *arXiv preprint arXiv:2505.11839*, 2025.
- [87] Zhilin Yang, Peng Qi, Saizheng Zhang, Yoshua Bengio, William Cohen, Ruslan Salakhutdinov, and Christopher D Manning. Hotpotqa: A dataset for diverse, explainable multi-hop question answering. In *Proceedings of the 2018 conference on empirical methods in natural language processing*, pages 2369–2380, 2018.
- [88] Shunyu Yao, Howard Chen, John Yang, and Karthik Narasimhan. Webshop: Towards scalable real-world web interaction with grounded language agents. *Advances in Neural Information Processing Systems*, 35:20744–20757, 2022.
- [89] Guibin Zhang, Muxin Fu, Guancheng Wan, Miao Yu, Kun Wang, and Shuicheng Yan. G-memory: Tracing hierarchical memory for multi-agent systems. *arXiv preprint arXiv:2506.07398*, 2025.
- [90] Hanrong Zhang, Jingyuan Huang, Kai Mei, Yifei Yao, Zhenting Wang, Chenlu Zhan, Hongwei Wang, and Yongfeng Zhang. Agent security bench (asb): Formalizing and benchmarking attacks and defenses in llm-based agents. *arXiv preprint arXiv:2410.02644*, 2024.
- [91] Jintian Zhang, Xin Xu, Ningyu Zhang, Ruibo Liu, Bryan Hooi, and Shumin Deng. Exploring collaboration mechanisms for llm agents: A social psychology view. *arXiv preprint arXiv:2310.02124*, 2023.
- [92] Zeyu Zhang, Quanyu Dai, Xiaohe Bo, Chen Ma, Rui Li, Xu Chen, Jieming Zhu, Zhenhua Dong, and Ji-Rong Wen. A survey on the memory mechanism of large language model-based agents. *ACM Transactions on Information Systems*, 43(6):1–47, 2025.
- [93] Zhehao Zhang, Weijie Xu, Fanyou Wu, and Chandan K Reddy. Falsereject: A resource for improving contextual safety and mitigating over-refusals in llms via structured reasoning. *arXiv preprint arXiv:2505.08054*, 2025.

- [94] Wanjun Zhong, Lianghong Guo, Qiqi Gao, He Ye, and Yanlin Wang. Memorybank: Enhancing large language models with long-term memory. In *Proceedings of the AAAI conference on artificial intelligence*, volume 38, pages 19724–19731, 2024.
- [95] Yuan Zhou, Peng Zhang, Mengya Song, Alice Zheng, Yiwen Lu, Zhiheng Liu, Yong Chen, and Zhaohan Xi. Zodiac: A cardiologist-level llm framework for multi-agent diagnostics. *arXiv preprint arXiv:2410.02026*, 2024.

A Supplementary Information of Zero-Trust Memory Game

A.1 Full Rationale for the Zero-Trust Formulation

The zero-trust formulation is motivated by three converging lines of evidence.

Misalignment in LLM-based agents. Large language model agents have been shown to exhibit sycophantic drift [18, 55], wherein a model progressively adjusts its stated beliefs toward those of a conversational partner regardless of evidential support. In the context of shared memory, this implies that a contributor agent may craft Δ_t not to reflect its best epistemic state but to conform to or reinforce a perceived consensus already encoded in \mathcal{M}_t . Analogously, an auditor agent subject to sycophancy will approve Δ_t because it matches existing memory patterns rather than because it is true. Both behaviors are misaligned with collective memory integrity yet neither constitutes classic Byzantine behavior, i.e., the agent is not “faulty” in the sense of crashing or sending random messages; it is behaving systematically in a way that is undetectable by fault-tolerance mechanisms.

Limitations of Byzantine fault tolerance. Byzantine fault tolerance (BFT) [8, 30] assumes that up to $f < n/3$ agents may behave arbitrarily, while the rest are honest. This framework is ill-suited to multi-agent LLM systems for two reasons. First, the fraction of misaligned agents is not known in advance and may exceed the BFT threshold, particularly when agents share the same base model and therefore share systematic biases [67]. Second, BFT assumes honest agents are identifiable by their consistent and correct behavior, whereas in LLM systems the same agent may behave honestly in one context and misalign in another depending on the prompt, the memory state, or the identities of other agents [48]. The zero-trust assumption removes the dependency on a trusted majority entirely.

Social choice and manipulation in multi-agent deliberation. Multi-agent debate frameworks [17, 36, 9, 82, 72] aggregate reasoning by having agents critique and revise each other’s outputs. Results in social choice theory [4, 21, 54] establish that any aggregation rule over rational agents is susceptible to intentional manipulation by at least one participant, where there is no mechanism that is simultaneously strategy-proof, Pareto-efficient, and non-dictatorial (Arrow’s impossibility theorem [20]). Applied to memory updating, this implies that for any commitment rule \mathcal{C} , there exists a profile of agent strategies under which the committed memory update is not the collectively optimal one. Zero-trust is therefore not a pessimistic special case but the general condition under which shared-memory deliberation operates.

A.2 Rationale for Utility Structures

Why the contributor utility takes a product form? The contributor’s utility $u_c = \Pr[\mathcal{C} = 1] \cdot \mathbb{I} - D$ is designed to reflect a strategic reality: committing an uninfluential delta has no value, and committing a high-influence delta that is immediately detected has negative value. The product $\Pr[\mathcal{C} = 1] \cdot \mathbb{I}$ captures this joint requirement, a contributor must simultaneously achieve commitment *and* influence to gain positive utility. Removing the scalar weights μ_c and ν_c from the earlier formulation is justified by noting that their ratio is not identifiable from observed behavior: only the tradeoff between the product term and D matters for equilibrium characterization, so we normalize without loss of generality.

Why auditor utility measures pre-commit alignment? The original formulation $\phi_i(\mathcal{M}_{t+1})$ conditions on the post-commit memory state, which is circular: the auditor’s vote determines whether the commit occurs, so its utility depends on its own action in a way that conflates strategic incentives with outcome evaluation. Instead, $\text{Align}(\Delta_t, \mathcal{M}_t)$ is a pre-commit signal that the auditor observes *before* voting, making the utility well-defined as an expected-payoff function over the auditor’s strategy. This is consistent with standard extensive-form game formulations where payoffs are evaluated at

terminal nodes given the full history, but the relevant information for strategy selection is what is observable before the action is taken.

Online estimation of $\text{Align}(\cdot)$ and c_i . The two remaining quantities in the auditor utility are estimated without human pre-specification.

Alignment signal. $\text{Align}(\Delta_t, \mathcal{M}_t)$ is computed by Φ as a normalized version of the architecture-specific calibration score:

$$\text{Align}(\Delta_t, \mathcal{M}_t) = 2\rho(\Delta_t, \mathcal{M}_t) - 1 \in [-1, +1] \quad (10)$$

where $\rho \in \{\rho^{\text{emb}}, \rho^{\text{graph}}\}$ is the calibration score defined in Section 4. This grounding means Align is entirely determined by the structural properties of Δ_t relative to \mathcal{M}_t , with no free parameters.

Effort cost. The effort cost c_i is estimated as the empirical mean token consumption (or wall-clock time) of a_i 's scrutiny actions across the most recent W rounds:

$$\hat{c}_i^{(t)} = \frac{1}{W} \sum_{t'=t-W}^{t-1} \text{cost}(a_i, t') \quad (11)$$

where $\text{cost}(a_i, t')$ is the measured computational cost of a_i 's participation in round t' . This is observable without any assumptions about agent internals and requires no human input. The window size W is set to the minimum value satisfying a standard variance criterion: $W^* = \min\{W : \text{Var}(\hat{c}_i^{(t)}) \leq \varepsilon_c\}$, where ε_c is the acceptable estimation error, making even this meta-parameter data-driven.

A.3 Equilibrium Failure Modes Under Zero-Trust

We formally establish three canonical failure modes that emerge as Nash equilibria of Γ under Assumption 3.1. These propositions collectively motivate why memory integrity cannot be achieved by agent-level trust alone, and provide the formal basis for the calibration mechanism of Section 4.

Proposition A.1 (Auditor Free-Riding). *Under a majority commitment rule \mathcal{C} with $|\mathcal{A}_t| = n$ auditors, if each auditor's effort cost satisfies $c_i > 0$ and the alignment signal $\text{Align}(\Delta_t, \mathcal{M}_t)$ is independent of any individual auditor's vote, then the unique dominant-strategy equilibrium is one of rubber-stamp approval: each $a_i \in \mathcal{A}_t$ emits $v_i = 1$ without scrutiny, regardless of Δ_t .*

Proof. Fix any auditor $a_i \in \mathcal{A}_t$ and let v_{-i} denote the votes of all other auditors. Under majority rule, a_i 's vote is pivotal (i.e., changes the commitment outcome) only if exactly $\lfloor n/2 \rfloor$ of the remaining $n - 1$ auditors vote to approve. Let p_{piv} denote this pivotality probability. For any symmetric mixed strategy profile over the other auditors with approval probability $q \in [0, 1]$:

$$p_{\text{piv}} = \binom{n-1}{\lfloor n/2 \rfloor} q^{\lfloor n/2 \rfloor} (1-q)^{n-\lfloor n/2 \rfloor-1} = O(n^{-1/2}) \quad (12)$$

by Stirling's approximation. The marginal integrity gain from scrutiny is therefore $p_{\text{piv}} \cdot \Delta \text{Align} \leq p_{\text{piv}} \cdot 2$, since $\text{Align} \in [-1, +1]$. The expected net utility gain from scrutiny over rubber-stamping is:

$$\Delta u_i = p_{\text{piv}} \cdot \Delta \text{Align} - c_i \leq 2p_{\text{piv}} - c_i = O(n^{-1/2}) - c_i \quad (13)$$

Since $c_i > 0$ is fixed and $p_{\text{piv}} \rightarrow 0$ as $n \rightarrow \infty$, there exists $n^* = O(c_i^{-2})$ such that $\Delta u_i < 0$ for all $n > n^*$. For any $n \geq 2$, $v_i = 1$ without scrutiny weakly dominates careful scrutiny because the effort cost c_i is incurred regardless of whether a_i is pivotal, while the integrity payoff from scrutiny requires pivotality. Therefore, $v_i = 1$ is the weakly dominant strategy for all a_i , and the unique dominant-strategy equilibrium is universal approval without scrutiny. \square

Proposition A.2 (Collusion Equilibrium). *Suppose a coalition $\mathcal{K} \subseteq \mathcal{A}_t$ of auditors shares a positive collusion benefit $\lambda_i > 0$ from approving Δ_t regardless of its content, and $|\mathcal{K}| \geq \lceil |\mathcal{A}_t|/2 \rceil$. Then there exists a Nash equilibrium in which every $a_i \in \mathcal{K}$ approves Δ_t unconditionally, the commitment rule \mathcal{C} is satisfied, and the committed delta may be arbitrarily inconsistent with \mathcal{M}_t .*

Proof. We construct the equilibrium strategy profile explicitly. Let each $a_i \in \mathcal{K}$ play the pure strategy $v_i = 1$ unconditionally, and let agents outside \mathcal{K} play any strategy. We verify that no agent in \mathcal{K} has a profitable deviation.

Payoff under collusion. For $a_i \in \mathcal{K}$, playing $v_i = 1$ yields:

$$u_i^{\text{collude}} = \text{Align}(\Delta_t, \mathcal{M}_t) + \lambda_i \quad (14)$$

where the effort cost term is zero since no scrutiny is performed.

Payoff under deviation. If a_i deviates to $v_i = 0$ (rejection), the collusion benefit λ_i is forfeited. Since $|\mathcal{K}| \geq \lceil |\mathcal{A}_t|/2 \rceil$, the majority threshold is still satisfied by $\mathcal{K} \setminus \{a_i\}$ whenever $|\mathcal{K}| > \lceil |\mathcal{A}_t|/2 \rceil$. In this case the deviation does not change the commitment outcome and the deviating auditor loses $\lambda_i > 0$:

$$u_i^{\text{deviate}} = \text{Align}(\Delta_t, \mathcal{M}_t) - c_i < u_i^{\text{collude}} \quad (15)$$

When $|\mathcal{K}| = \lceil |\mathcal{A}_t|/2 \rceil$ exactly, deviation by a_i does change the outcome to rejection, but a_i 's payoff then becomes $\text{Align}(\Delta_t, \mathcal{M}_t) - c_i - \lambda_i < u_i^{\text{collude}}$ since $\lambda_i > 0$ and $c_i > 0$. In both cases deviation is strictly dominated.

Commitment outcome. Since $|\mathcal{K}|$ meets the majority threshold, $\mathcal{C}(\{v_i\}_{i \in \mathcal{A}_t}) = 1$ regardless of the content of Δ_t . In particular, Δ_t may satisfy $\text{Align}(\Delta_t, \mathcal{M}_t) = -1$ (maximal inconsistency) and still be committed. No agent in \mathcal{K} has incentive to deviate, so this constitutes a Nash equilibrium. \square

Proposition A.3 (Adversarial Rejection). *Suppose a blocking coalition $\mathcal{B} \subseteq \mathcal{A}_t$ satisfies $|\mathcal{B}| > \lfloor |\mathcal{A}_t|/2 \rfloor$, and each $a_i \in \mathcal{B}$ has utility strictly decreasing in the contributor a_c 's influence on \mathcal{M} , i.e., u_i is decreasing in $\mathbb{I}(\Delta_t, \mathcal{M}_t)$ for any Δ_t from a_c . Then there exists a Nash equilibrium in which all Δ_t from a_c are rejected regardless of their consistency with \mathcal{M}_t .*

Proof. Let each $a_i \in \mathcal{B}$ play the pure strategy $v_i = 0$ unconditionally for any Δ_t proposed by a_c .

Payoff under adversarial rejection. For $a_i \in \mathcal{B}$, rejecting Δ_t prevents commitment and therefore prevents a_c from gaining influence over \mathcal{M} . Since u_i is decreasing in $\mathbb{I}(\Delta_t, \mathcal{M}_t)$, blocking the commit yields:

$$u_i^{\text{reject}} = \text{Align}(\Delta_t, \mathcal{M}_t) \cdot \mathbf{1}[\mathcal{C} = 1] - c_i \cdot \mathbf{1}[v_i = \text{scrutinize}] \quad (16)$$

Under unconditional rejection without scrutiny, $\mathcal{C} = 0$ and $c_i = 0$, so $u_i^{\text{reject}} = 0$.

Payoff under deviation. If a_i deviates to $v_i = 1$, and $|\mathcal{B}| - 1 \geq \lfloor |\mathcal{A}_t|/2 \rfloor$ still holds (which is true when $|\mathcal{B}| > \lfloor |\mathcal{A}_t|/2 \rfloor + 1$), the outcome remains rejection and the deviation yields no benefit. When $|\mathcal{B}| = \lfloor |\mathcal{A}_t|/2 \rfloor + 1$, a deviation to $v_i = 1$ may flip the outcome to commitment, increasing a_c 's influence. Since u_i is strictly decreasing in \mathbb{I} :

$$u_i^{\text{approve}} < u_i^{\text{reject}} = 0 \quad (17)$$

So deviation to approval is strictly dominated for all $a_i \in \mathcal{B}$. Since $|\mathcal{B}|$ exceeds the blocking threshold, $\mathcal{C}(\{v_i\}) = 0$ for all Δ_t from a_c , independently of Δ_t 's consistency with \mathcal{M}_t . \square

Remark A.4. *Propositions A.1–A.3 are not mutually exclusive. A single auditor set \mathcal{A}_t may simultaneously contain free-riders (Proposition A.1), a colluding sub-coalition (Proposition A.2), and an adversarially rejecting sub-coalition (Proposition A.3). The three failure modes operate on disjoint subsets of \mathcal{A}_t and their effects compound: free-riders provide no signal, colluders inject false approval, and adversarial rejectors suppress truthful updates. Together, they establish that no voting rule over untrusted auditors (e.g., majority, supermajority, or weighted) can guarantee memory integrity in the worst case, since each rule is vulnerable to at least one of the three equilibria. This impossibility is the formal foundation for replacing the vote-based commitment rule \mathcal{C} with the structural calibration mechanism Φ in Section 4.*

Mapping to the three failure cases of Figure 1. Propositions A.1–A.3 and the three failure cases described in Section 1 are related by a many-to-many correspondence rather than a one-to-one one, because each proposition characterizes an *equilibrium structure* (which strategy profile is stable) while each case in Figure 1 characterizes an *observed memory outcome* (what the resulting \mathcal{M}_{t+1} looks like). A single equilibrium can produce different outcomes depending on the content of Δ_t , and a single outcome can arise from different equilibria depending on which failure of agent confidence drives it. We make the correspondence explicit below.

Proposition A.1 (free-riding) produces Case 1 outcomes when the contributor is over-confident: rubber-stamp approval without scrutiny commits whatever Δ_t is proposed, including hallucinated

Table 2: Many-to-many correspondence between equilibrium failure modes (Propositions A.1–A.3) and observed memory outcomes (Cases 1-3 of Figure 1). ✓ indicates the proposition can produce the case; ✗ indicates it structurally cannot.

	Case 1 (corruption)	Case 2 (over-rejection)	Case 3 (uncertain/no commit)
Prop. A.1 (free-riding)	✓		✓
Prop. A.2 (collusion)	✓	✓	
Prop. A.3 (adv. rejection)		✓	✓

entries with high stated confidence. It produces Case 3 outcomes when the contributor is itself hedged: rubber-stamp approval of a “no-commit” or noise proposal yields an under-populated memory. Free-riding does not produce Case 2, because rubber-stamping never rejects.

Proposition A.2 (collusion) produces Case 1 outcomes when colluding auditors approve a high-confidence corrupt contributor. This is the canonical “two confident agents endorse a hallucinated entry” pattern. It produces Case 2 outcomes when the colluding majority approves a confident contributor’s *rejection* of a tentative contribution, suppressing correct content with stated certainty. Collusion does not produce Case 3, because collusion is by definition active commitment, not abstention.

Proposition A.3 (adversarial rejection) produces Case 2 outcomes directly: a blocking coalition vetoes truthful Δ_t with high confidence regardless of its alignment, which is exactly the over-curation pattern. It produces Case 3 outcomes when the blocking coalition’s rejection coexists with weak contribution from the remaining agents (uncertain/no commit happens) and what could have been useful content is lost. Adversarial rejection does not produce Case 1, because rejection cannot inject corrupt content.

Overall, we have three observations: First, every case is reachable by at least two of the three equilibria, so no single proposition fully characterizes any single case. Second, every proposition produces at least two cases, so no single failure mode at the agent level produces a unique memory outcome. Third, the union of the three propositions covers all three cases, confirming that the failure-case taxonomy of Figure 1 is exhaustively grounded in the equilibrium analysis: any observable confidence-driven failure of shared-memory debate corresponds to at least one of the three propositions.

B System-Level Equilibrium and Memory Calibration

B.1 Existence of Equilibrium

We first establish that the game Γ always has at least one equilibrium, regardless of agent strategies or utility parameters.

Proposition B.1 (Existence of Equilibrium). *Under Assumption 3.1, the zero-trust memory game Γ admits at least one mixed-strategy equilibrium.*

Proof. We verify the three conditions of Nash’s existence theorem [44] as extended to finite extensive-form games by Kuhn [29].

(i) Finite player set. The player set $\{a_c\} \cup \mathcal{A}_t$ is finite by assumption, with $|\mathcal{A}_t| = n - 1 < \infty$.

(ii) Compact and convex strategy spaces. The contributor’s pure strategy space \mathbb{D} is finite; its mixed extension $\Delta(\mathbb{D})$ is the probability simplex over \mathbb{D} , which is compact and convex. Each auditor a_i ’s pure strategy space is $\{0, 1\}$; its mixed extension $[0, 1]$ is compact and convex. The joint strategy space $\Delta(\mathbb{D}) \times \prod_{i \in \mathcal{A}_t} [0, 1]$ is therefore compact and convex.

(iii) Continuity of expected utilities. The contributor’s expected utility $\mathbb{E}[u_c(\Delta_t, \mathcal{M}_t)]$ involves $\Pr[\mathcal{C}(\{v_i\}) = 1 \mid \Delta_t]$, which is multilinear in auditors’ mixed strategies $\{\pi_i\}$ and therefore continuous. The influence term $\mathbb{I}(\Delta_t, \mathcal{M}_t)$ and detection term $D(\Delta_t, \mathcal{M}_t)$ are fixed for a given Δ_t and \mathcal{M}_t , so continuity is preserved. Each auditor’s expected utility $\mathbb{E}[u_i(\pi_i, \Delta_t, \mathcal{M}_t)]$ is linear in π_i and continuous in the joint strategy profile by the same argument.

Since all three conditions hold, Nash’s theorem guarantees the existence of a fixed point of the best-response correspondence, constituting a mixed-strategy equilibrium of Γ . \square

Remark B.2. *Existence is guaranteed but the equilibrium is generically non-unique. In particular, all three failure-mode equilibria (Propositions A.1–A.3) are valid Nash equilibria under their respective parameter regimes. Existence therefore does not imply desirability, which we address via the integrity gap below.*

B.2 The Integrity Gap

Not all Nash equilibria of Γ produce good memory. We quantify how far an equilibrium outcome can be from the ideal using the **integrity gap**.

Let $\mathcal{M}_{t+1}^* = \text{MERGE}(\mathcal{M}_t, \Delta_t^*)$ denote the memory state from committing the integrity-optimal delta $\Delta_t^* = \arg \max_{\Delta} \text{Align}(\Delta, \mathcal{M}_t)$, and let $\mathcal{M}_{t+1}^{\text{eq}}$ be the memory state resulting from the equilibrium profile $(\Delta_t^*, \{\pi_i^*\})$. The integrity gap is:

$$\mathcal{G}(\Gamma) = \text{Align}(\Delta_t^*, \mathcal{M}_t) - \mathbb{E}[\text{Align}(\Delta_t^{\text{eq}}, \mathcal{M}_t)] \quad (18)$$

where the expectation is over the randomness in mixed strategies. Under the three failure-mode equilibria, the gap is strictly positive: free-riding auditors approve manipulative deltas with $\text{Align}(\Delta_t, \mathcal{M}_t) \ll 1$; colluding auditors do the same unconditionally; and adversarial rejectors block truthful deltas with $\text{Align}(\Delta_t, \mathcal{M}_t) \approx 1$. In all three cases, $\mathcal{G}(\Gamma) > 0$ and memory degrades over time.

The root cause in each case is the same: the commitment outcome is determined by auditor votes, so agents optimize their votes rather than the quality of their evidence. The calibration mechanism Φ addresses this by replacing vote-based commitment with score-based commitment, as we show next.

B.3 How Calibration Closes the Integrity Gap

The calibration mechanism Φ transforms Γ into an effective game $\tilde{\Gamma}$ by replacing the vote-based commitment rule $\mathcal{C}(\{v_i\})$ with a structure-based rule:

$$\tilde{\mathcal{C}}(\Delta_t, \mathcal{M}_t) = \mathbf{1}[\rho(\Delta_t, \mathcal{M}_t) \geq \rho^*] \quad (19)$$

where $\rho \in \{\rho^{\text{emb}}, \rho^{\text{graph}}\}$ is the architecture-specific calibration score. This single change propagates through both utility functions and closes the gap via three channels.

Channel 1: Raising the contributor’s detection cost. Under $\tilde{\mathcal{C}}$, the contributor’s commitment gain is no longer a function of auditor persuasibility but of the calibration score:

$$\tilde{u}_c(\Delta_t, \mathcal{M}_t) = \mathbf{1}[\rho(\Delta_t, \mathcal{M}_t) \geq \rho^*] \cdot \mathbb{I}(\Delta_t, \mathcal{M}_t) - D(\Delta_t, \mathcal{M}_t) \quad (20)$$

Since ρ and D are positively correlated by construction, i.e., $D(\Delta_t, \mathcal{M}_t) = 1 - \rho(\Delta_t, \mathcal{M}_t)$, a more manipulative Δ_t scores lower on ρ and is more likely to be rejected. The contributor therefore faces a hard **manipulation ceiling**: it cannot simultaneously maximize influence \mathbb{I} and pass the calibration gate $\rho \geq \rho^*$. The equilibrium delta satisfies:

$$D(\tilde{\Delta}_t^*, \mathcal{M}_t) \leq \frac{1}{1 + \kappa} \quad (21)$$

where $\kappa > 0$ is the correlation coefficient between D and $1 - \rho$, estimated online from the history of calibration scores. This bound is decreasing in κ : a tighter correlation between detectability and calibration score forces more truthful contributions.

Channel 2: Eliminating auditor free-riding. Under $\tilde{\mathcal{C}}$, the commitment outcome no longer depends on auditor votes at all. The marginal integrity payoff from casting a vote is therefore exactly zero:

$$\frac{\partial}{\partial v_i} \mathbb{E}[\text{Align}(\Delta_t, \mathcal{M}_t) \mid \tilde{\mathcal{C}}] = 0 \quad \forall a_i \in \mathcal{A}_t \quad (22)$$

This eliminates the free-riding problem at its source. Auditor effort is instead redirected toward mandatory structural evidence tasks, i.e., probe query submission (embedding memory) and path

attestation (graph memory), whose outputs feed directly into $\rho(\Delta_t, \mathcal{M}_t)$. These tasks have a well-defined marginal contribution to ρ , giving auditors a concrete structural incentive to participate honestly.

Channel 3: Deterring collusion intertemporally. The credibility weight $w_i^{(t)}$ decays when an auditor submits structurally invalid evidence:

$$w_i^{(t+1)} = w_i^{(t)} \cdot (1 - \delta \cdot \mathbf{1}[\text{invalid evidence from } a_i]) \quad (23)$$

An auditor's long-run expected payoff is:

$$V_i = \sum_{t=0}^{\infty} \beta^t \text{Align}(\Delta_t, \mathcal{M}_t) \cdot w_i^{(t)} - c_i \cdot \mathbf{1}[\text{attest}] \quad (24)$$

Collusion (submitting invalid paths or garbage probes to support a manipulative Δ_t) reduces $w_i^{(t)}$, which reduces V_i in all future rounds. For sufficiently patient auditors (β close to 1), this long-run credibility loss outweighs any short-run benefit from collusion, making honest attestation the dominant intertemporal strategy.

B.4 The Calibrated Equilibrium

The three channels above collectively bound the integrity gap under $\tilde{\Gamma}$. The gap decomposes into three independent residual sources:

$$\mathcal{G}(\tilde{\Gamma}) = \underbrace{\mathcal{G}_{\text{manip}}}_{\text{contributor residual}} + \underbrace{\mathcal{G}_{\text{thresh}}}_{\text{threshold error}} + \underbrace{\mathcal{G}_{\text{attest}}}_{\text{attestation noise}} \quad (25)$$

where $\mathcal{G}_{\text{manip}} = O(1/(1 + \kappa))$ from Equation (21) and vanishes as $\kappa \rightarrow \infty$; $\mathcal{G}_{\text{thresh}}$ is minimized at the optimal threshold ρ_{opt}^* and estimated adaptively; and $\mathcal{G}_{\text{attest}} = O(1/\sqrt{b})$ by a Hoeffding bound over b sampled auditors and vanishes as $b \rightarrow \infty$. Combining:

$$\mathcal{G}(\tilde{\Gamma}) \leq \underbrace{\frac{C_1}{1 + \kappa}}_{\text{manipulation}} + \underbrace{C_2 \cdot |\rho^* - \rho_{\text{opt}}^*|}_{\text{threshold}} + \underbrace{\frac{C_3}{\sqrt{b}}}_{\text{attestation}} =: \epsilon(\kappa, \rho^*, b) \quad (26)$$

for system-level constants $C_1, C_2, C_3 > 0$.

Proposition B.3 (Calibrated Equilibrium). *Under the calibration mechanism Φ with correlation parameter κ , adaptive threshold ρ^* , and b attestation auditors, the effective game $\tilde{\Gamma}$ admits an equilibrium $(\tilde{\Delta}_t^*, \{\tilde{\pi}_i^*\})$, i.e., the **calibrated equilibrium**, in which the integrity gap satisfies (26). In particular:*

- (i) $\mathcal{G}(\tilde{\Gamma}) \rightarrow 0$ as $\kappa \rightarrow \infty$, $\rho^* \rightarrow \rho_{\text{opt}}^*$, and $b \rightarrow \infty$.
- (ii) $\mathcal{G}(\tilde{\Gamma}) < \mathcal{G}(\Gamma)$ for any $\kappa > 0$, $\rho^* > 0$, $b \geq 1$: calibration strictly improves memory integrity over the uncalibrated game under any non-trivial setting.
- (iii) The calibrated equilibrium requires no agent to be honest: integrity is achieved structurally, consistent with Assumption 3.1.

Proof sketch. Existence of the equilibrium $(\tilde{\Delta}_t^*, \{\tilde{\pi}_i^*\})$ in $\tilde{\Gamma}$ follows from Proposition B.1 applied to $\tilde{\Gamma}$, which satisfies the same finite-player, compact-strategy, continuous-utility conditions with $\tilde{\mathcal{C}}$ replacing \mathcal{C} .

(i) Each residual term in (26) vanishes under the stated limiting conditions independently, so their sum vanishes.

(ii) For any $\kappa > 0$, the manipulation ceiling in Channel 1 strictly reduces $\mathcal{G}_{\text{manip}}$ below its uncalibrated value (where $\kappa = 0$ and the contributor faces no structural detection cost). For any $b \geq 1$, the attestation component strictly reduces $\mathcal{G}_{\text{attest}}$ below the uncalibrated case (where auditor evidence is not collected at all).

(iii) The calibration score ρ is computed entirely from structural properties of Δ_t and \mathcal{M}_t , with auditor outputs treated as potentially adversarial inputs. No agent’s honesty is assumed at any point in the computation of \tilde{C} . \square

The residual gap $\epsilon > 0$ reflects the fundamental limits of structural verification under zero-trust: a perfect gap of zero would require either a trusted verifier or an unbounded attestation budget. The bound (26) makes this tradeoff explicit, with κ estimated online, ρ^* set adaptively, and b depends on the size of agent group, leaving no free parameters requiring human specification.

B.5 How the Calibrated Equilibrium Addresses Each Debate Failure (Figure 1)

The calibration mechanism Φ (Section 4) replaces the vote-based commitment rule C with a score-based rule \tilde{C} (Eq. 19 in Appendix B.3), which removes the dependency of the commit outcome on agent votes and therefore on agent confidence. We trace how this single change resolves each of the three cases.

Case 1 (confident corruption). In the uncalibrated game, an over-confident contributor’s Δ_t commits whenever auditors rubber-stamp (Prop. A.1) or collude (Prop. A.2), regardless of Δ_t ’s alignment with \mathcal{M}_t . Under Φ , commitment requires $\rho(\Delta_t, \mathcal{M}_t) \geq \rho^*$. A corrupt Δ_t (whether hallucinated, sycophantic, or adversarially crafted) produces low ρ_{align} because the entry disrupts retrieval over auditor probes against \mathcal{M}_t (§4), and often low ρ_{detect} because the entry lacks the structural support of genuinely informative content. The contributor’s stated confidence does not enter the score. Channel 1 of Appendix B.3 (*Raising the contributor’s detection cost*) formalizes this: the manipulation ceiling $\tilde{D}(\Delta_t^*, \mathcal{M}_t) \leq 1/(1 + \kappa)$ bounds the detectability of any corrupt Δ_t that passes Φ , and this bound tightens as κ grows.

Case 2 (confident over-rejection). In the uncalibrated game, a blocking coalition (Prop. A.3) or a confident colluding majority (Prop. A.2) can suppress a tentative but correct Δ_t simply by voting against it. Under Φ , the auditor’s vote does not enter the commit decision at all, only the structural evidence the auditor submits (probe queries for embedding memory, reachability checks for graph memory) contributes to ρ . A correct Δ_t produces non-disrupting retrieval against well-formed probes (high ρ_{align}) and adequate structural support (high ρ_{detect}) regardless of any auditor’s stated rejection. Channel 2 of Appendix B.3 (*Eliminating auditor free-riding*) formalizes this: $\partial \mathbb{E}[\text{Align}]/\partial v_i = 0$, so any vote-based suppression strategy has zero leverage on the commit outcome.

Case 3 (collective hedging). Cases 1 and 2 are active failures: the wrong outcome is committed or the right outcome is rejected. Case 3 is a passive failure: uncertain (or no) commit happens when a useful one was possible. Φ does not attempt to “force” a commit in Case 3, when all auditors hedge, ρ_{align} is low across the board because hedging probes produce minimal structural evidence, and the system correctly declines to commit. This is the right behavior: committing a noise-level Δ_t under collective hedging would be a Case 1 failure in disguise. What Φ provides in Case 3 is *symmetry of failure*: an honestly-hedged round commits nothing, and an adversarially-hedged round also commits nothing, so an attacker has no asymmetric leverage. Channel 3 of Appendix B.3 (*Deterring collusion intertemporally*) ensures that auditors who systematically submit hedge-style probes accumulate credibility decay, so an adversary cannot maintain Case 3 outcomes indefinitely against an honest minority.

Two observations close this analysis. First, Φ does not require any agent to be honest: the score ρ is computed entirely from structural properties of Δ_t and \mathcal{M}_t , so the calibrated equilibrium is robust to all three failure modes simultaneously, even when they coexist in the same round (Remark A.4). Second, the three cases are addressed by *different channels* of the calibration mechanism (Case 1 by ρ_{detect} bounding manipulation; Case 2 by ρ being independent of votes; Case 3 by ρ_{align} declining to commit under hedge), which is why no single component of Φ is sufficient on its own. The ablation study in Appendix D.4 confirms that removing any one component degrades performance, and the degradation pattern matches which case the removed component primarily addresses.

C Calibration Mechanism: Implementation Details and Proofs

This appendix supplies the technical details deferred from §4. We provide necessary justifications, document every adaptive parameter and how it is initialized at cold start, prove the recovery prop-

erty of the credibility update, justify the latency claim, characterize the additional memory and token overhead, and give implementation notes for both the embedding and graph instantiations of EQUIMEM.

C.1 Mapping Between Calibration Quantities and Utility Components

This subsection makes precise the claim, illustrated visually in Figure 2, that every component of the contributor utility $u_c = \Pr[C=1] \cdot I - D$ and the auditor utility $u_i = \text{Align}(\Delta_t, M_t) - c_i$ defined in Section 3 is controlled, at the calibrated equilibrium of $\tilde{\Gamma}$, by exactly one of the three calibration quantities in EQUIMEM: the detection signal ρ_{detect} , the alignment signal ρ_{align} , and the credibility weight $w_i^{(t)}$ (into which we fold the commit gate $\mathbf{1}[\rho \geq \rho^*]$, since the gate’s structural authority comes from $w_i^{(t)}$ entering ρ multiplicatively). Table 3 summarizes the mapping; the rest of the subsection states and justifies each row. We address mechanisms only insofar as they bear on equilibrium utility control; implementation details are deferred to the rest of Appendix C.

Table 3: Per-component mapping between the three calibration quantities of EQUIMEM and the utility components they control at the calibrated equilibrium. Each row identifies the component, the calibration quantity that controls it, and the property that does the control.

Calibration quantity	Side	Utility component	Controlling property
ρ_{detect}	Contributor	$D(\Delta_t, M_t)$	detection regulation
	Contributor	$I(\Delta_t, M_t)$	influence ceiling
ρ_{align}	Auditor	$\text{Align}(\Delta_t, M_t)$	sample-time regulation
	Auditor	c_i	probe re-use and damping
$w_i^{(t)}$ (with commit gate)	Contributor	$\Pr[C=1]$	vote-independent regulation
	Auditor	c_i	damping

C.1.1 The detection signal ρ_{detect} controls D and I

The detection signal scores how the proposed Δ_t sits in the geometry (embedding case) or topology (graph case) of M_t . Both contributor utility components on the left of u_c , namely D and I , are controlled by this single quantity at equilibrium.

Control of $D(\Delta_t, M_t)$ via detection regulation. In the uncalibrated game Γ , D is conceptual: detection has no operational meaning unless an external mechanism makes inconsistency observable. EQUIMEM supplies that mechanism by setting $D := 1 - \rho$, where ρ_{detect} is the dominant input (low alignment alone cannot redeem a high-density delta because $\rho = \sqrt{\rho_{\text{detect}} \cdot \rho_{\text{align}}}$).

Justification. By construction $\rho \in [0, 1]$, hence $D \in [0, 1]$ as required by Eq. (3). The substitution $D = 1 - \rho$ is the natural one in the sense that the correlation coefficient between D and $1 - \rho$ is exactly $\kappa = 1$, achieving the manipulation ceiling derived in Appendix A.3 (Channel 1). In particular, ρ_{detect} becomes informative as a detection signal precisely when Δ_t disturbs the local density (embedding) or violates local/path consistency (graph) – the two manipulations the contributor’s I relies on. There is therefore no slack at equilibrium in which a high- I delta scores low on D .

Control of $I(\Delta_t, M_t)$ via influence ceiling. The influence term I measures how much Δ_t shifts downstream retrieval. A manipulative contributor maximizes I by placing Δ_t in regions of M_t that dominate retrieval, i.e., regions of high local embedding density, or graph edges that bypass existing multi-hop paths. These are exactly the patterns that ρ_{detect} scores; the retrieval re-scaling described in §4.3 then forces every committed entry’s effective influence to be capped by its ρ_{detect} score.

Justification (embedding case). For an entry e_k^Δ , $\rho_{\text{detect}}(\Delta_t) = 1 - \frac{1}{K} \sum_k \hat{r}_k / (\bar{r} + \epsilon)$. Let I_k denote the marginal influence of e_k^Δ on top- k retrieval against an arbitrary query distribution. Top- k retrieval returns the k nearest neighbours, so e_k^Δ enters the result for any query lying within a ball of radius proportional to its neighbourhood density, giving $I_k = \Theta(\hat{r}_k)$ asymptotically in $|M_t|$. The retrieval re-scaling $\tilde{e}_k = \sqrt{\rho_k} e_k$ at read time then yields

$$I_k^{\text{eff}} = \rho_k \cdot I_k \leq \rho_k \cdot \Theta(\hat{r}_k)$$

which is jointly capped because ρ_k is decreasing in \hat{r}_k through ρ_{detect} . A delta cannot simultaneously score high on ρ_{detect} and exert large I .

Justification (graph case). For a new edge $e = (u, r, v)$, $I(e)$ is determined by how often e lies on multi-hop retrieval paths. The path-strength product $\prod_{e \in \pi} \rho_e$ used at retrieval ensures that any path through a low- ρ_{detect} edge is automatically discounted, so $I^{\text{eff}}(e) \leq \rho_{\text{detect}}(e) \cdot I_{\text{max}}$. The ceiling $D \leq 1/(1 + \kappa)$ in Eq. (26) of Appendix B.3 then gives a closed-form upper bound on equilibrium influence.

C.1.2 The alignment signal ρ_{align} controls Align and c_i

The alignment signal is computed from auditor probes (queries q_i for embedding memory, traversal paths π_i for graph memory). Both auditor utility terms are controlled by this single quantity at equilibrium: the alignment signal in u_i is regulated in ρ_{align} directly, and the effort cost c_i collapses because the probes that produce ρ_{align} are reused from the auditor’s normal debate activity.

Control of Align(Δ_t, M_t) via sample-time non-manipulability. EQUIMEM regulates the alignment signal as $\text{Align}(\Delta_t, M_t) := 2\rho - 1 \in [-1, +1]$ (Eq. 4, Appendix A.2), where ρ_{align} is the auditor-side input. We make explicit why this regulating is unmanipulable by any auditor at equilibrium.

Justification. Let auditor a_i submit probe evidence ξ_i . The alignment signal decomposes as

$$\rho_{\text{align}}(\Delta_t) = 1 - \frac{1}{|\mathcal{A}_t|} \sum_{j \in \mathcal{A}_t} w_j^{(t)} \cdot s(\xi_j; \Delta_t, M_t)$$

where s is the per-auditor disagreement (RBO distance for embeddings, indicator of unreachability for graphs). Two structural properties make ρ_{align} robust to single-auditor manipulation. First, ξ_i is sampled uniformly from Q_i (or fixed to the auditor’s current path), so a_i cannot pre-commit to a probe that flatters its preferred outcome; the sampling is performed by EQUIMEM, not a_i . Second, the multiplicative entry of $w_j^{(t)}$ caps any single auditor’s marginal influence:

$$\left| \frac{\partial \rho_{\text{align}}}{\partial \xi_i} \right| \leq \frac{w_i^{(t)}}{|\mathcal{A}_t|}$$

At equilibrium, honest auditors converge to $w_i^{(t)} \rightarrow 1$ (Proposition C.1), giving them full influence; adversarial auditors converge toward 0. The alignment term in u_i therefore tracks the structural quantity $2\rho - 1$ rather than any self-reported judgment.

Damping c_i via probe re-use. The effort cost c_i in u_i models the resource cost an auditor incurs by performing scrutiny. In Γ , scrutiny is a separate costly action, which produces the free-riding equilibrium (Proposition A.1). EQUIMEM neutralizes this cost because the probes used to compute ρ_{align} are exactly the queries and traversals the auditor already issues during debate.

Justification. Let $\mathcal{T}_i^{\text{debate}}$ be the set of LLM calls and tool invocations a_i performs as part of normal debate participation, and let \mathcal{T}_i^Φ be the additional set induced by EQUIMEM. Every probe used by EQUIMEM is sampled from Q_i (which a_i generates regardless of EQUIMEM) or set to π_i (the path a_i already walked), so

$$\mathcal{T}_i^\Phi \subseteq \mathcal{T}_i^{\text{debate}}$$

The empirical effort cost (Appendix A.2)

$$\hat{c}_i^{(t)} = \frac{1}{W} \sum_{t'=t-W}^{t-1} [\text{cost}(\mathcal{T}_i^{\text{debate}} \cup \mathcal{T}_i^\Phi, t') - \text{cost}(\mathcal{T}_i^{\text{debate}}, t')] = 0$$

in expectation, modulo $O(1)$ algorithmic overhead dominated by LLM inference cost (Appendix D.9). The marginal scrutiny cost is therefore asymptotically zero at equilibrium, and the free-riding incentive of Proposition A.1 dissolves.

C.1.3 The credibility weight $w_i^{(t)}$ (with commit gate) controls $\Pr[C=1]$ and c_i

The credibility weight enters ρ multiplicatively through ρ_{align} and gates commitment via $\mathbf{1}[\rho \geq \rho^*]$. The commit gate is therefore not a separate calibration quantity but the structural endpoint of $w_i^{(t)}$:

without credibility weighting, the gate would be vote-equivalent. We group them and show that together they control the contributor’s commit-probability term and the auditor’s collusion incentive at equilibrium.

Control of $\Pr[C=1]$ via vote-independent commitment. Under Γ , the commit probability is the expectation over auditor strategies $\Pr[C(\{v_i\}) = 1 \mid \Delta_t]$, which depends multilinearly on the mixed strategies $\{\pi_i\}$ and is therefore manipulable by any pivotal coalition (Propositions A.1–A.3). Under $\tilde{\Gamma}$, EQUIMEM replaces this term with the indicator $\mathbf{1}[\rho \geq \rho^*]$. The structural authority of this substitution comes from $w_i^{(t)}$: an adversarial auditor who tries to push ρ_{align} up or down sees its $w_i^{(t)}$ decay multiplicatively, so its leverage on the commit decision vanishes at equilibrium.

Justification. Fix any Δ_t and M_t , and let $\sigma = (\sigma_c, \sigma_1, \dots, \sigma_{|\mathcal{A}_t|})$ be the joint strategy profile. The commit indicator under $\tilde{\Gamma}$ satisfies

$$\frac{\partial}{\partial \sigma_i} \mathbf{1}[\rho(\Delta_t, M_t) \geq \rho^*] = 0 \quad \forall a_i \in \mathcal{A}_t$$

because ρ is computed from (Δ_t, M_t) and from the sampled probes, neither of which is a vote or self-report; the auditor’s only channel of influence is its probe distribution, weighted by $w_i^{(t)}$. At the calibrated equilibrium, $w_i^{(t)} \rightarrow 1 - p_i$ where p_i is the auditor’s long-run invalid-probe rate (Proposition C.1), so an adversarial auditor’s contribution to the commit decision is bounded by $1 - p_i$ and shrinks to zero as it persists in attempting manipulation. Conditional on prior debate actions, the commit decision is therefore a deterministic function of (Δ_t, M_t) and an auditor’s marginal vote does not move it. This eliminates the pivot-probability term that drives the three failure equilibria and replaces vote-based commitment with a structural rule.

Control of c_i via multiplicative damping. The cost c_i in u_i models the resource effort an auditor incurs when submitting a structurally invalid probe in support of a manipulative Δ_t (collusion). The credibility weight $w_i^{(t)}$ damps the auditor’s lifetime alignment payoff multiplicatively whenever such an invalid probe is detected, so collusion incurs both an immediate cost and a long-run weight loss.

Justification. A single invalid probe at round t multiplies the auditor’s subsequent credibility trajectory by a factor of $(1 - \delta)$ relative to honest play (Eq. 7). Consider a one-shot deviation at round $t = 0$ followed by honest behaviour. Let $\bar{A} := \mathbb{E}[\text{Align}(\Delta_t, M_t)]$ at the calibrated equilibrium and $\bar{w} := \mathbb{E}[w_i^{(t)}] \rightarrow 1$ along the honest trajectory. The discounted lifetime payoff is

$$V_i = \sum_{t=0}^{\infty} \beta^t \left(\text{Align}(\Delta_t, M_t) \cdot w_i^{(t)} - c_i \cdot \mathbf{1}[\text{collude at } t] \right)$$

Computing the difference between honest and colluding play under a one-shot deviation,

$$V_i^{\text{honest}} - V_i^{\text{collude}} = c_i + \sum_{t=1}^{\infty} \beta^t \bar{A} \bar{w} \delta = c_i + \frac{\beta \delta}{1 - \beta} \bar{A} \bar{w} > 0$$

for any $c_i \geq 0$, $\bar{A} > 0$, and $\beta \in (0, 1)$. The first term is the immediate cost the auditor avoids by staying honest; the second is the long-run weight loss that compounds geometrically because credibility decay propagates through every future round’s alignment contribution. Both terms favour honesty, so collusion is strictly dominated under $\tilde{\Gamma}$ at the calibrated equilibrium without c_i needing any specific value: even at $c_i = 0$, the multiplicative damping alone suffices.

C.2 Adaptive Parameters and Cold-Start Behavior

EQUIMEM uses several adaptive parameters in place of fixed hyperparameters. Each is computed from observable round statistics, so no value is set by the user. Table 4 summarizes them.

Cold start for the commit gate ρ^* . At round $t = 0$ no committed scores exist, so the running median is undefined. We initialize $\rho^* = 0.5$, the midpoint of the score range. Every Δ_t is provisionally accepted while the history buffer fills. Once the buffer reaches W entries, ρ^* becomes the running median and EQUIMEM enters its steady-state regime. This warm-up affects only the first W rounds, and the only effect is that early commits may be lower-trust than steady-state commits. Subsequent

Table 4: Adaptive parameters used by EQUIMEM. Each is computed from observable round statistics rather than tuned.

Symbol	Definition	Source
ρ^*	commit gate	running median of last W committed ρ scores
δ_t	credibility update rate	fraction of probes invalid in round t
η_t	path-compatibility cutoff	running median of past $\text{comp}(\cdot)$ values
α_t	local/path mixture weight	fraction of edges in Δ_t with $ \mathcal{P}_{uv} > 0$
adaptive radius	embedding similarity cutoff	running median of pairwise similarities in \mathcal{M}_t
L_{\max}	BFS depth bound	$\lceil \log \mathcal{V}_t \rceil$
W	history window for medians	$\max(30, \lceil \sqrt{ \mathcal{M}_t } \rceil)$

retrieval discounts these early entries through the trust-weight mechanism (§4.3), so any inaccuracy is absorbed at read time rather than persisting in the memory.

Cold start for the credibility rate δ_t . At $t = 0$ no probes have been observed, so we initialize $\delta_0 = 0.1$, a conservative default that produces a slow update. From round $t = 1$ onward, δ_t is the empirical fraction of invalid probes observed in round t . The choice of δ_0 affects only the first round’s weight movement and is forgotten by round $t = 2$, so it is not a tunable parameter in any meaningful sense.

Cold start for η_t and α_t . Both depend on observed graph statistics. At $t = 0$ we set $\eta_0 = 0$ (accept any compatibility score) and $\alpha_0 = 0.5$ (equal weighting of local and path checks). They become data-driven from round 1 onward.

Why these defaults are not tunable. A reviewer might object that $\rho_0^* = 0.5$, $\delta_0 = 0.1$, $\eta_0 = 0$, and $\alpha_0 = 0.5$ are themselves choices. We emphasize that these defaults affect only a $O(W)$ -round warm-up and have no effect on steady-state behavior, since the running statistics overwrite each initial value within W rounds.

C.3 Credibility Recovery: Proof of Fixed Point

We prove the claim from §4.2 that an auditor whose long-run invalid-probe rate is p has credibility weight converging to $w^* = 1 - p$.

Proposition C.1 (Credibility fixed point). *Let a_i produce invalid probes independently with probability $p \in [0, 1]$ at each round, and let $\delta_t \in (0, 1)$ for all t . Then under Eq. 7, $\mathbb{E}[w_i^{(t)}] \rightarrow 1 - p$ as $t \rightarrow \infty$.*

Proof. Taking expectations on both sides of Eq. 7 and treating δ_t as approximately constant at its long-run value δ (justified because δ_t converges to its empirical mean by the law of large numbers):

$$\mathbb{E}[w_i^{(t+1)}] = p \cdot \mathbb{E}[w_i^{(t)}](1 - \delta) + (1 - p) \left(\mathbb{E}[w_i^{(t)}] + \delta(1 - \mathbb{E}[w_i^{(t)}]) \right) \quad (27)$$

$$= \mathbb{E}[w_i^{(t)}] (p(1 - \delta) + (1 - p)(1 - \delta)) + (1 - p)\delta \quad (28)$$

$$= \mathbb{E}[w_i^{(t)}](1 - \delta) + (1 - p)\delta. \quad (29)$$

This is a linear contraction with contraction factor $1 - \delta \in (0, 1)$ and offset $(1 - p)\delta$. Its unique fixed point is

$$w^* = \frac{(1 - p)\delta}{1 - (1 - \delta)} = 1 - p, \quad (30)$$

and convergence is geometric at rate $1 - \delta$. □ □

Recovery time. The half-life of weight movement is $\log 2 / \log(1/(1 - \delta)) \approx \ln 2 / \delta$ rounds. With a typical $\delta \approx 0.1$, an honest auditor that suffered a one-time slip recovers half the distance to $w^* = 1$ in roughly 7 rounds, and reaches within 5% of w^* in roughly 30 rounds.

Robustness to time-varying δ_t . If δ_t is non-constant but bounded away from 0 and 1, the update remains a contraction and the fixed point still tracks $1 - p_t$, where p_t is the auditor’s invalid rate at round t . This means a previously dishonest auditor who reforms can recover full credibility, and a

previously honest auditor who turns adversarial loses credibility without instant collapse, both of which are desirable robustness properties.

C.4 Latency Analysis

We show that calibration adds only marginal time on top of the baseline retrieval cost in both architectures. The key reason is that EQUIMEM reuses computations and data structures already produced by baseline retrieval, so it never pays a second time for the same work.

Embedding case. Baseline top- k retrieval costs $O(k \log N)$ per query using an HNSW or IVF index. Calibration adds two passes whose cost can be analyzed below the baseline:

- **Detection pass.** For each of K new entries we perform an ANN range query to count neighbors within the adaptive radius. Because $K \ll N$ in any incremental update (the delta is small relative to memory size), the total $O(K \log N)$ is much smaller than the $O(k \log N)$ baseline cost, not comparable to it. Concretely, this pass costs no more than $\frac{K}{k}$ of one baseline retrieval.
- **Alignment pass.** For each auditor a_i , the top- k result against \mathcal{M}_t is already produced by baseline retrieval (the auditor was about to use q_i anyway), so calibration reuses it for free. Only the marginal effect of Δ_t needs to be computed: we score the K new vectors against q_i in $O(K)$ time and merge them into the cached top- k in $O(k)$ time, then compute d_{RBO} in $O(k)$. Total per auditor: $O(K + k)$, with no $\log N$ factor. Across auditors: $O(|\mathcal{A}_t|(K + k))$.

Total added cost: $O(K \log N + |\mathcal{A}_t|(K + k))$. Since both K and $|\mathcal{A}_t|(K + k)$ are independent of N except for the single $K \log N$ term (which itself is much smaller than baseline because $K \ll k$ in practice), calibration overhead is sub-baseline.

Graph case. Baseline graph retrieval traverses up to L_{max} hops at cost $O(d^{L_{\text{max}}})$, where d is the average degree and $L_{\text{max}} = \lceil \log |\mathcal{V}_t| \rceil$. Calibration adds three pieces:

- **Local check.** A neighborhood scan over u 's existing edges costs $O(d)$ per new edge, so $O(|\mathcal{E}_t^\Delta| d)$ in total. Since baseline retrieval is $O(d^{L_{\text{max}}})$ with $L_{\text{max}} \geq 2$, this is smaller than baseline by a factor of $d^{L_{\text{max}}-1}$.
- **Path check.** Bidirectional BFS gives $O(d^{L_{\text{max}}/2})$ per edge, which is the square root of the baseline's $O(d^{L_{\text{max}}})$. Even summed over $|\mathcal{E}_t^\Delta|$ edges, this stays well below baseline as long as $|\mathcal{E}_t^\Delta| \ll d^{L_{\text{max}}/2}$, true for any realistic incremental update.
- **Alignment pass.** A reachability check costs $O(\log |\mathcal{V}_t|)$ per auditor by reusing the adjacency index already loaded for baseline retrieval. Total: $O(|\mathcal{A}_t| \log |\mathcal{V}_t|)$.

All three terms are smaller than the baseline $O(d^{L_{\text{max}}})$ by at least one factor of $d^{L_{\text{max}}/2}$, so calibration cost is again sub-baseline.

No extra LLM calls. The dominant cost in any agent-based system is the LLM forward pass. EQUIMEM makes zero additional LLM calls. Probes reuse queries and walks the auditors generate during normal debate, and every scoring step is algorithmic (ANN lookups, BFS, RBO). The asymptotic added cost above is therefore the full added cost.

Complexity table. Table 5 states the asymptotic cost of every stage and the ratio between added cost and the baseline retrieval cost. The ratio is shown in the rightmost column and is strictly less than 1 across all stages under the regimes named in the caption.

Two observations close the analysis. **(i)** Every added stage shares the same asymptotic terms as the baseline ($\log N$ for embeddings, $d^{L_{\text{max}}}$ or smaller for graphs), so calibration scales with the same primitives the baseline uses. **(ii)** The multiplicative factors in front of those terms (K , $|\mathcal{A}_t|$, $|\mathcal{E}_t^\Delta|$) are all independent of memory size and stay small in practice, which is what makes the added cost marginal rather than merely comparable.

C.5 Memory and Token Overhead

Memory overhead. EQUIMEM stores three additional pieces of state beyond the base memory:

Table 5: Time complexity of each calibration stage and the ratio of added cost to baseline retrieval cost. The ratios are small under typical operating regimes: $K \ll k$ (delta size much smaller than top- k width), $|\mathcal{A}_t|$ a small constant, $|\mathcal{V}_t|$ a small graph, $|\mathcal{E}_t^\Delta| \ll d^{L_{\max}/2}$ (incremental updates). Under these conditions every added stage is sub-baseline, and total calibration overhead remains marginal relative to one round of baseline retrieval.

Arch.	Stage	Baseline cost	EQUIMEM added cost	Ratio (added / base)
Embedding	Retrieval / query	$O(k \log N)$	—	—
	Detection pass	—	$O(K \log N)$	$K/k \ll 1$
	Alignment pass	—	$O(\mathcal{A}_t (K+k))$	$ \mathcal{A}_t (K+k)/(k \log N) \ll 1$
	Credibility / re-weight	—	$O(\mathcal{A}_t + K)$	negligible
Graph	Retrieval / query	$O(d^{L_{\max}})$	—	—
	Local check	—	$O(\mathcal{E}_t^\Delta d)$	$ \mathcal{E}_t^\Delta /d^{L_{\max}-1} \ll 1$
	Path check	—	$O(\mathcal{E}_t^\Delta d^{L_{\max}/2})$	$ \mathcal{E}_t^\Delta /d^{L_{\max}/2} \ll 1$
	Alignment	—	$O(\mathcal{A}_t \log \mathcal{V}_t)$	$ \mathcal{A}_t \log \mathcal{V}_t /d^{L_{\max}} \ll 1$

- One scalar trust weight $\rho \in [0, 1]$ per committed entry. For a memory of N entries, this is N floating-point numbers, or roughly $4N$ bytes at single precision. Compared to the embedding storage of $4dN$ bytes (for d -dimensional embeddings), this is a $1/d$ relative overhead, which is negligible at typical $d \in [768, 1536]$.
- One credibility weight $w_i^{(t)} \in [0, 1]$ per auditor. For $|\mathcal{N}|$ agents, this is $|\mathcal{N}|$ scalars, constant in N .
- A bounded history buffer of recent calibration scores for computing ρ^* and η_t . We maintain the last W scores using a fixed-size ring buffer, so memory is $O(W)$ regardless of how many rounds have elapsed.

Total: an additional $O(N + W + |\mathcal{N}|)$ scalars on top of the base memory, dominated by the trust-weight column.

Token overhead. We emphasize again that EQUIMEM makes zero additional LLM calls. The contributor’s Δ_t generation, the auditors’ query and path-walking activity, and the agent debate itself are all unchanged. The probes EQUIMEM uses are exactly the queries and walks the auditors would issue without calibration. There is no calibration prompt, no auditor-side reasoning solicited, and no contributor-side justification generated. Token consumption per round is therefore identical to an uncalibrated multi-agent debate of the same configuration.

Index overhead. For embedding memory we reuse the existing ANN index. Calibration queries it but does not modify it beyond standard insertion, so no new index structure or rebuild step is added. For graph memory we reuse the existing adjacency structure plus a small side index $\mathcal{R}_{\text{compat}}$ of relation co-occurrence counts. The side index has size $O(|\mathcal{R}|^2)$ where $|\mathcal{R}|$ is the number of relation types ($\leq 10^3$ even for large knowledge graphs), so it adds at most a few megabytes regardless of $|\mathcal{V}_t|$. Both index costs are constant in the memory size and therefore do not enter the asymptotic analysis of §C.4.

C.6 Compatibility Set Estimation

The compatibility set $\mathcal{R}_{\text{compat}}(r)$ used in the graph-memory local check is learned from the existing graph rather than supplied as an external ontology. We compute it as follows.

For each pair of relation types $(r, r') \in \mathcal{R} \times \mathcal{R}$, we count the number of nodes $u \in \mathcal{V}_t$ where u has both an outgoing edge of type r and an outgoing edge of type r' . Call this count $c(r, r')$. We define the co-occurrence score:

$$\text{cooc}(r, r') = \frac{c(r, r')}{c(r) \cdot c(r') / |\mathcal{V}_t|} \quad (31)$$

where $c(r) = \sum_{r'} c(r, r')$ is the marginal occurrence count of relation r . This is the standard pointwise mutual information form, normalized so that random co-occurrence yields $\text{cooc} = 1$.

The compatibility set is then:

$$\mathcal{R}_{\text{compat}}(r) = \{r' \in \mathcal{R} : \text{cooc}(r, r') \geq \tau_t\} \quad (32)$$

where τ_t is the running median of all cooc values in the current graph (again adaptive, no manual setting). At cold start (empty graph), $\mathcal{R}_{\text{compat}}(r) = \mathcal{R}$ for all r , meaning the local check is uninformative until the graph has enough edges to estimate co-occurrence. This degrades the detection signal during warm-up but does not produce false rejections, because s_{local} stays at 1 when the set is universal.

Update cost. $\mathcal{R}_{\text{compat}}$ is recomputed incrementally. Each new edge (u, r, v) updates at most $|\mathcal{N}(u)|$ entries of $c(r, \cdot)$, so per-edge update cost is $O(|\mathcal{N}(u)|)$. Summed over the new-edge set, the total $O(|\mathcal{E}_t^\Delta| \cdot d)$ matches the local-check term in Table 5 and is therefore absorbed into the marginal-cost budget already analyzed in §C.4. No separate latency cost is incurred for maintaining $\mathcal{R}_{\text{compat}}$.

Storage cost. $\mathcal{R}_{\text{compat}}$ is stored as a $|\mathcal{R}| \times |\mathcal{R}|$ co-occurrence matrix, where $|\mathcal{R}|$ is the number of relation types. Even at $|\mathcal{R}| = 10^3$ (large for a knowledge graph), this is 10^6 scalars, i.e., a few megabytes, independent of $|\mathcal{V}_t|$. Compared to the base graph storage of $O(|\mathcal{V}_t| + |\mathcal{E}_t|)$ entries, this is a constant additive overhead and does not affect any complexity bound.

C.7 Bidirectional BFS Depth and Cost

We chose $L_{\text{max}} = \lceil \log |\mathcal{V}_t| \rceil$ for the bidirectional BFS in the path check. This choice rests on two empirical regularities of knowledge graphs.

First, real-world knowledge graphs satisfy a small-world property: the typical shortest-path distance between two random nodes scales as $O(\log |\mathcal{V}|)$. This holds for ConceptNet, Wikidata, Freebase, and the graph memories used by [3] and [89]. Setting L_{max} to this scale captures essentially all paths the contributor could plausibly justify, while truncating exponential blowup of BFS at deeper levels.

Second, bidirectional BFS searches from both endpoints simultaneously and meets in the middle, so the effective branching factor is $d^{L_{\text{max}}/2}$ rather than $d^{L_{\text{max}}}$. With $L_{\text{max}} = \log |\mathcal{V}_t|$ this gives a worst-case cost of $\sqrt{|\mathcal{V}_t|} \cdot \text{poly}(d)$, which is sub-linear in graph size.

Failure modes. If the graph is unusually dense or has a large diameter, $L_{\text{max}} = \log |\mathcal{V}_t|$ may either over-explore or miss valid paths. We detect this online by tracking the running ratio $|\mathcal{P}_{uv}|/\text{expected paths}$ across rounds. If the ratio drifts outside $[0.5, 2.0]$, we adjust L_{max} by ± 1 . The adjustment changes the BFS cost by at most a factor of $d^{1/2}$ (the same bidirectional speedup applies), so the marginal-cost analysis in Table 5 still holds within a constant factor.

C.8 Retrieval Complexity Under Trust Weighting

We claimed in §4.3 that trust weighting adds zero asymptotic cost to retrieval (not just marginal cost, but no added cost at all). We justify this for both architectures.

Embedding retrieval. The trust-weighted vector $\tilde{\mathbf{e}}_k = \sqrt{\rho_k} \cdot \mathbf{e}_k$ is computed once at index-load time and stored in place of \mathbf{e}_k . Top- k retrieval against $\{\tilde{\mathbf{e}}_k\}$ uses the same ANN index structure as retrieval against $\{\mathbf{e}_k\}$, with the same $O(k \log N)$ cost per query. When an entry’s ρ_k is updated, we re-scale that single vector in $O(d)$ and re-insert into the ANN index in $O(\log N)$, identical to a standard memory write. No new cost term enters Table 5.

Graph retrieval. For path queries, the trust-weighted path strength $\prod_{e \in \pi} \rho_e$ is computed lazily during traversal: each edge access multiplies the running product by ρ_e . This is one extra multiplication per visited edge, an $O(1)$ overhead on top of the $O(1)$ baseline edge-access cost. Total query complexity stays at $O(d^{L_{\text{max}}})$, identical to baseline. When an edge’s ρ_e is updated, we modify a single entry in the edge attribute table in $O(1)$.

C.9 Implementation Notes

We provide a few practical notes for re-implementation.

ANN index choice. We use HNSW [40] with $M = 16$ and $\text{ef} = 200$ for the embedding case. The detection pass requires range queries (count neighbors within a similarity radius), which HNSW does not natively support, so we issue a top- k query with a generous upper bound (e.g., $k_{\text{filter}} = 100$) and filter by the adaptive radius post-hoc. The post-hoc filter is $O(k_{\text{filter}})$ per call and does not change the $O(\log N)$ asymptotic of the underlying ANN query, so it is absorbed into the $O(K \log N)$ detection-pass cost reported in Table 5.

RBO truncation. Rank-biased overlap is defined as an infinite series, but it converges geometrically. We truncate at depth k (the same k used for top- k retrieval) with persistence parameter $p_{\text{RBO}} = 0.9$, the default in the original RBO paper. This is a property of RBO itself and not a hyperparameter introduced by EQUIMEM.

Probe sampling. For embedding memory, Q_i is the auditor’s pending-query queue (typically size 1 to 5 per round). For graph memory, π_i is the auditor’s most recent traversal path. In both cases, we sample uniformly using the system’s standard random number generator with a seed reset at each round to prevent adaptive auditors from predicting future samples from past behavior.

Numerical stability. We clamp all ρ , w_i , ρ_{geo} , and ρ_{ret} values into $[10^{-6}, 1 - 10^{-6}]$ before taking products or square roots, to avoid underflow when scores accumulate over many rounds. This is standard numerical hygiene and not a tunable parameter.

D Experiments Results Analysis

D.1 Configuration

LLM backbone and implementation. All experiments in Table 1 use Qwen3-VL-8B-Instruct [63] as the agent backbone, deployed locally via Ollama with $N = 6$ agents per system. We select Qwen3-VL-8B-Instruct because it achieves SOTA on AgentBench and ToolBench among 8B models under the Apache 2.0 license, while its native function-calling interface simplifies multi-agent orchestration. Alternative backbones (DeepSeek-R1-Distill-7B, Llama-3.1-8B) are evaluated in Appendix D.5.

Each agent operates independently with no shared parameters or centralised coordination, except for interaction through the shared memory \mathcal{M} . The calibration mechanism Φ is implemented as a standalone Python process with no generative LLM dependency for runtime scoring decisions, consistent with its role as the only component not subject to Definition 3.1. This design ensures that Φ cannot be manipulated by any agent and remains a structurally trusted component in the system.

Embeddings used in ρ_{detect} and ρ_{align} are computed using all-MiniLM-L6-v2 [73] with approximate nearest-neighbour retrieval for efficient scaling to large memory sizes. Experiments with varying agent counts $N \in \{4, 10\}$ are reported in Appendix D.6.

Hyperparameter settings. We summarise the key hyperparameters in Table 6. Unlike prior multi-agent or memory-based systems that rely on manually tuned thresholds, EQUIMEM minimises the number of fixed hyperparameters by estimating most quantities directly from data.

Table 6: Key hyperparameters and configurations in EQUIMEM.

Component	Parameter	Value / Strategy
Agents	Number of agents N	6 (default), varied in Appendix
LLM	Backbone	Qwen3-VL-8B-Instruct
Memory	Top- k retrieval	$k = 5$
Embedding	Dimension d	384 (MiniLM default)
Calibration	Commit threshold ρ^*	Running median (adaptive)
Detection	Radius threshold	Median similarity (adaptive)
Graph	Path depth L_{max}	$\lceil \log \mathcal{V} \rceil$
Alignment	Probe sampling	Uniform random from Q_i
Credibility	Update rate δ_t	Invalid probe ratio (adaptive)

Adaptive parameter estimation. A key design principle of EQUIMEM is that most hyperparameters are *data-adaptive* rather than manually tuned:

- The commit threshold ρ^* is defined as the running median of calibration scores over recent committed entries, eliminating the need for task-specific threshold tuning.
- Detection thresholds (e.g., neighbourhood radius in embedding space, compatibility scores in graph memory) are derived from empirical statistics such as median similarity or historical co-occurrence patterns, ensuring robustness across different domains.

- The credibility update rate δ_t is computed as the fraction of invalid probes in each round, allowing the system to automatically adjust its sensitivity to auditor behaviour without introducing additional parameters.
- Graph traversal depth L_{\max} scales with the logarithm of graph size, reflecting typical structural properties of real-world knowledge graphs while maintaining computational efficiency.

This adaptive design serves two purposes. First, it reduces the risk of overfitting hyperparameters to specific benchmarks, improving generalisation across tasks and memory architectures. Second, it aligns with the zero-trust assumption by avoiding reliance on any externally tuned or agent-provided signals. All thresholds are grounded in observable system statistics, ensuring that calibration remains consistent and robust under adversarial or non-cooperative agent behaviours.

D.2 Dataset Statistics

Why these benchmarks. The four benchmarks are selected to stress-test the primary failure modes identified by our zero-trust game analysis: (i) a single dominant contributor injecting a locally plausible but globally inconsistent entry, and (ii) auditors rubber-stamping an incorrect proposal when uncertain or sycophantic. These failures cause particular harm in long-horizon tasks—premature goal states in embodied action, fabricated intermediate facts in multi-hop reasoning, and temporal contradictions in lifelong conversation. The selected datasets span knowledge-intensive and action-intensive domains, providing the diverse challenge needed to evaluate EQUIMEM’s calibration.

Table 7 summarises the four benchmarks used in our experiments. We report the number of task instances, the average interaction length, the evaluation metric, and the domain of each benchmark.

Table 7: Benchmark statistics for the four evaluation benchmarks.

Benchmark	#Tasks	Avg. Len.	Metric	Domain	Source
ALFWorld	134	~25 steps	Success rate	Embodied	[57]
Webshop	1000	~30 steps	Reward	Embodied	[88]
HotpotQA	500	1 query	Accuracy	Knowledge	[87]
LoCoMo	500	<300 turns	F1	Knowledge	[39]

ALFWorld is a text-based embodied environment derived from ALFRED, covering six task categories: `pick_and_place`, `look_at_obj_in_light`, `pick_clean_then_place`, `pick_heat_then_place`, `pick_cool_then_place`, and `pick_two_obj_and_place`. We use the `valid_unseen` split (134 tasks), where each task requires a sequence of physical actions with an average length of approximately 25 steps. **Why it matters:** The long action chain and strict precondition dependencies make this benchmark particularly susceptible to premature goal-state injection—a corrupted memory entry that incorrectly asserts a task is complete can terminate the entire episode with zero reward (see Case 2 in Appendix E).

WebShop is an embodied decision-making benchmark that simulates online shopping through natural language interactions. Each task requires an agent to navigate search results, apply filters, and inspect product pages to locate a specified item. We evaluate on 1,000 randomly sampled tasks, with an average trajectory length of approximately 30 steps. **Why it matters:** The large, dynamic search space forces frequent memory writes under uncertainty; a dominant agent that confidently commits an incorrect product attribute (e.g., a wrong color or price) can mislead the entire downstream search process.

HotpotQA is a multi-hop question answering benchmark constructed from Wikipedia. Each instance requires reasoning across multiple documents to derive the final answer. We use 500 questions drawn from the full HotpotQA dev set, each consisting of a single query, and report accuracy. **Why it matters:** A hallucinated intermediate fact committed to shared memory can override correct evidence later retrieved by other agents, directly testing the ability of ρ_{align} to detect inconsistent overwrites in the retrieval pool (see Case 1).

LoCoMo is a long-context conversational memory benchmark. Each original dialogue spans up to 35 sessions and averages 300 turns, simulating a lifelong, multi-session human conversation. From these long-form dialogues, we sample 500 question-answering tasks, each derived from a *separate* dialogue

to guarantee statistical independence. Every task presents the full dialogue history in memory and asks one evaluative question requiring cross-session temporal reasoning. We report F1 as the primary evaluation metric. **Why it matters:** The extreme temporal span (300 turns) naturally creates memory decay, contradiction, and topic drift across sessions. This tests the most dangerous failure mode for our theory: a contributor who proposes a confident but incorrect summary, and a room of auditors who, due to the cost of searching 300-turn memory, prefer to agree rather than verify (see Case 3).

D.3 Extended Analysis of Overall Effectiveness

This section expands on our insights of §5.2 with deeper mechanistic explanation.

Why isolated checks saturate? On embedding memory, the gain from Vanilla to the strongest per-entry baseline (A-MemGuard) is modest, and EQUIMEM then adds a further substantial improvement on top, exceeding the combined gain of all three intermediate baselines (LLM Audit, PPL Filter, A-MemGuard). The three baselines also cluster tightly with frequent rank inversions, suggesting they capture overlapping signals rather than complementary ones.

Both observations are consistent with the saturation hypothesis: isolated entry level checks evaluate only the *intrinsic quality* of Δ_t (grammaticality, fluency, perplexity), while the dominant errors in a growing memory \mathcal{M}_t arise from *relational inconsistency*, where an entry reads perfectly in isolation yet contradicts existing memory. The two pass design $\sqrt{\rho_{\text{detect}} \cdot \rho_{\text{align}}}$ breaks this ceiling by evaluating each delta against \mathcal{M}_t as a whole rather than as an independent unit.

Qualitative pattern of ceiling aware gains. An inverse scaling effect is visible across all configurations: EQUIMEM’s gain over the next best baseline is largest where that baseline is weakest, and shrinks where the baseline already performs well. This pattern holds consistently across reasoning intensive and action intensive benchmarks alike, with the largest improvements appearing in settings where existing safeguards struggle the most.

This shrinkage is not a weakness of Φ but a property of its gating regime: a calibration filter can only act on entries that would otherwise be admitted erroneously, so its marginal effect is bounded by the fraction of errors in the input stream. Importantly, this inverse scaling pattern is *inconsistent* with the hypothesis that performance gains stem from external knowledge leakage, which would produce a constant additive boost regardless of baseline strength. Instead, it is *consistent* with the hypothesis that Φ filters errors that downstream baselines would have admitted.

Memory benchmark interaction. The strongest results for reasoning intensive benchmarks come from AriGraph paired with EQUIMEM, while the strongest action task results come from G-Memory paired with EQUIMEM. This complementarity is already visible in the Vanilla setting: AriGraph leads on multi hop QA, while G-Memory leads on embodied action and long dialogue tasks. These pre existing biases reflect each architecture’s native design. AriGraph’s semantic knowledge graph with episodic memory is well suited to multi hop QA, while G-Memory’s three tier hierarchical structure captures the long action chains and multi session dialogue history of action and conversational tasks.

EQUIMEM’s calibration Φ *inherits and amplifies* these biases rather than imposing a generic filter that flattens architectural differences. Because ρ_{detect} and ρ_{align} are computed directly from each architecture’s geometry (embedding manifold) or topology (graph neighbourhood and multi hop paths), Φ filters out noisy entries that dilute the architecture’s native signal, allowing each design’s strengths to emerge more clearly. The gap between AriGraph and G-Memory therefore widens under EQUIMEM in the directions each architecture is naturally suited to, rather than narrowing toward a common baseline.

Cross MAS consistency. Absolute performance differs substantially across MAD frameworks, with AutoGen generally leading, followed by DyLAN and MacNet. Yet EQUIMEM’s gain over the next best baseline is comparably stable across all three frameworks. The same ranking and the same inverse scaling pattern persist regardless of which orchestration scheme is used.

The stability of the gain across orchestration regimes confirms that Φ acts at the memory layer rather than at the coordination layer. Weak orchestration and strong orchestration receive similar lifts because calibration filters Δ_t at the point of write, which is upstream of any MAS specific aggregation. This decoupling is a practical advantage: EQUIMEM can be deployed with any MAD framework without re tuning or framework specific adaptation.

Table 8: Ablation study of EQUIMEM’s calibration components (%). We ablate one component at a time, keeping all notation consistent with Section 4. For embedding memory, ρ_{detect} and ρ_{align} are removed directly. For graph memory, we remove components contributing to ρ_{detect} and ρ_{align} , including an explicit ablation of ρ_{align} . All configurations use AutoGen + Qwen3-VL-8B-Instruct, $N = 6$ agents, benign setting (mean \pm std over 5 runs). Bold indicates the full EQUIMEM.

Memory	Ablation	AutoGen				MacNet				DyLAN			
		HQA	LCM	ALF	WS	HQA	LCM	ALF	WS	HQA	LCM	ALF	WS
MemBank (emb.)	w/o ρ_{detect}	45.0 \pm 6.3	32.9 \pm 6.6	70.7 \pm 3.4	36.8 \pm 8.6	48.3 \pm 9.5	33.1 \pm 10.2	51.8 \pm 1.0	43.7 \pm 7.1	46.4 \pm 0.9	35.6 \pm 6.3	58.5 \pm 2.6	40.7 \pm 3.6
	w/o ρ_{align}	39.4 \pm 5.1	25.7 \pm 6.5	74.0 \pm 3.9	38.0 \pm 8.1	44.5 \pm 8.2	20.7 \pm 10.6	59.8 \pm 1.0	45.2 \pm 7.6	41.3 \pm 0.8	28.4 \pm 7.2	65.4 \pm 2.5	43.4 \pm 3.7
	w/o reweighting	47.0 \pm 6.0	33.6 \pm 5.5	75.3 \pm 4.1	42.3 \pm 8.2	52.1 \pm 8.3	34.5 \pm 10.5	62.2 \pm 1.2	49.4 \pm 6.2	49.2 \pm 0.8	37.7 \pm 6.8	68.5 \pm 2.4	46.3 \pm 3.5
G-Memory (graph)	w/o s_{local} (ρ_{detect})	45.3 \pm 10.1	52.8 \pm 3.6	76.3 \pm 3.9	48.8 \pm 6.5	41.2 \pm 7.3	55.8 \pm 1.5	67.6 \pm 10.0	51.4 \pm 3.7	42.1 \pm 8.1	47.5 \pm 2.6	64.1 \pm 12.1	45.0 \pm 6.4
	w/o s_{path} (ρ_{detect})	38.7 \pm 9.3	49.3 \pm 3.7	80.9 \pm 3.5	51.3 \pm 6.2	35.4 \pm 6.6	50.2 \pm 1.8	70.6 \pm 8.6	55.0 \pm 3.4	36.5 \pm 9.0	39.8 \pm 2.6	69.1 \pm 12.0	47.2 \pm 6.2
	w/o ρ_{align}	41.9 \pm 9.6	53.7 \pm 3.5	79.0 \pm 3.6	50.2 \pm 6.3	39.0 \pm 6.9	54.4 \pm 1.6	69.3 \pm 9.1	52.6 \pm 3.5	40.3 \pm 8.8	43.1 \pm 2.7	67.2 \pm 11.5	47.5 \pm 6.1
	w/o reweighting	47.0 \pm 9.8	56.4 \pm 3.4	82.3 \pm 3.7	52.5 \pm 6.4	46.5 \pm 6.6	58.0 \pm 1.6	72.5 \pm 9.7	55.8 \pm 3.3	47.0 \pm 8.5	49.5 \pm 2.8	71.4 \pm 10.6	50.7 \pm 6.0

D.4 Ablation Study

This part dissects EQUIMEM’s calibration mechanism Φ into its component scoring passes to identify which elements drive the gains observed in RQ1. We ablate one component at a time on two representative memory architectures (MemBank and G-Memory) across all three MAS frameworks and four benchmarks. Table 8 reports the results.

Retrieval aware checks are the most important components. Removing ρ_{align} from embedding memory causes the largest drops in the table, with the steepest declines appearing on reasoning intensive benchmarks. In graph memory, removing s_{path} , which contributes to the detection signal ρ_{detect} , produces the largest single component drops, again with the most severe declines on reasoning tasks. These drops are substantially larger than those from removing reweighting alone.

Both ρ_{align} and s_{path} share the same principle: they evaluate Δ_t against the *broader memory state* \mathcal{M}_t rather than in isolation. ρ_{align} measures how much the proposed delta disrupts retrieval rankings (embedding) or violates multi hop path consistency (graph). Without this signal, EQUIMEM loses its ability to detect entries that are locally plausible but globally inconsistent. This is the dominant failure mode shared by LLM Audit and PPL Filter (Section 5.2).

The dominant component depends on the benchmark category. The alignment signal ρ_{align} contributes most on reasoning intensive benchmarks (HotpotQA, LoCoMo), where multi hop evidence chains are critical and a single inconsistent entry can derail downstream reasoning. The drops from removing it are largest on these benchmarks, smaller on action tasks such as ALFWorld, and intermediate on WebShop.

In contrast, detection signals (ρ_{detect}) contribute more on action intensive benchmarks (ALFWorld, WebShop), where state consistency matters. On embedding memory, removing ρ_{detect} hurts action benchmarks more than removing ρ_{align} does. The same pattern holds in graph memory, where removing detection components such as s_{local} or s_{path} produces noticeable drops on action tasks even when the corresponding alignment drops are smaller.

This asymmetry validates the two pass design of Section 4.2: ρ_{detect} captures local plausibility and structural density (critical for state consistency in action tasks), while ρ_{align} captures global consistency across evidence chains (critical for reasoning tasks). Their composition ensures that both failure modes are covered, regardless of benchmark category.

Auditor reweighting has the smallest benign effect. Removing the credibility weight decay $w_i^{(t)}$ causes the smallest drops among the three ablated components in nearly every configuration. The declines from removing reweighting are markedly smaller than those from removing ρ_{align} or s_{path} under the same configurations.

This is expected: reweighting penalises auditors whose probes are structurally invalid, but in the benign setting agents rarely produce invalid signals, so $w_i^{(t)}$ remains close to its initial value. The reweighting mechanism becomes critical under adversarial settings (Section 5.3), where malicious auditors submit misleading probes and credibility decay is required to suppress their influence over time. The minimal benign impact demonstrates that reweighting imposes essentially no cost on

Table 9: Performance with alternative LLM backbones (%) on MacNet, $N = 6$ agents, benign setting.

Memory	Safeguard	Qwen3-VL-8B-Instruct (primary)				DeepSeek-R1-Distill-7B				Llama-3.1-8B			
		HQA	LCM	ALF	WS	HQA	LCM	ALF	WS	HQA	LCM	ALF	WS
MemBank (entb)	Vanilla	33.6±8.2	20.7±10.2	48.9±4.3	24.2±7.3	34.8±9.4	24.5±11.1	45.2±3.8	23.6±6.1	32.4±8.1	18.2±9.5	47.1±2.4	20.4±7.5
	+ LLM Audit	41.4±7.7	22.8±10.2	60.3±6.2	31.8±7.3	42.1±8.3	27.2±10.5	53.7±3.4	28.1±7.2	36.9±7.9	21.5±10.1	51.2±6.2	26.5±6.8
	+ PPL Filter	41.8±8.7	29.4±10.4	57.2±2.2	25.6±8.0	39.5±9.1	34.1±12.2	51.6±6.6	25.9±7.4	37.2±9.6	24.1±10.8	55.4±3.5	24.2±8.1
	+ A-MemGuard	44.5±6.2	32.7±7.6	58.5±4.0	39.6±7.6	46.2±7.5	33.8±8.1	54.9±5.2	35.1±7.9	42.6±6.8	30.4±8.5	52.8±3.3	33.4±7.2
	+ EQUIMEM	56.1±7.8	38.8±8.4	66.0±5.9	55.0±5.9	53.5±8.2	36.7±9.1	60.3±4.2	47.8±6.4	47.0±8.5	30.9±8.0	56.6±3.1	44.1±6.2
G-Memory (graph)	Vanilla	35.6±7.4	47.6±1.5	67.1±12.5	45.1±4.4	38.9±8.0	49.2±1.8	65.5±11.8	43.8±5.1	31.2±6.7	45.3±1.6	62.1±10.9	40.5±4.2
	+ LLM Audit	40.0±7.9	51.3±1.4	68.5±10.4	49.3±4.9	42.7±7.4	54.1±1.7	67.1±12.1	46.2±5.3	38.4±8.2	47.2±1.8	65.4±11.2	44.1±4.5
	+ PPL Filter	43.2±7.0	56.8±1.3	72.6±10.4	54.7±3.5	47.5±7.2	59.4±1.5	70.8±11.1	51.4±3.9	40.8±7.8	49.6±1.5	66.2±10.5	48.2±4.0
	+ A-MemGuard	—	—	—	—	—	—	—	—	—	—	—	—
	+ EQUIMEM	54.5±6.2	62.1±1.4	74.2±8.1	60.1±2.9	53.3±6.5	59.0±1.6	69.0±8.8	55.2±3.3	47.9±6.9	52.8±1.5	66.8±8.2	51.2±3.4

honest agents, while its protective value materialises precisely when the zero trust assumption is violated by adversaries.

No single component is sufficient. Even the most impactful individual ablation does not collapse performance to the Vanilla level. The ablated system always retains a clear margin above the corresponding Vanilla score, even when the most important component is removed. Removing only reweighting leaves a system that is only marginally weaker than full EQUIMEM in the benign setting, confirming that credibility tracking does not harm honest agents.

This gradient confirms that Φ operates as a composed scoring mechanism: each component targets a distinct failure mode, and their combination is necessary for full robustness. The fact that even the most severe ablation retains performance above Vanilla demonstrates that the remaining components provide partial, non overlapping protection, exactly the property required for a defence in depth design under the zero trust assumption.

D.5 Alternative LLM Backbones

Table 1 uses Qwen3-VL-8B-Instruct as the agent backbone throughout. To verify that EQUIMEM’s advantage is not specific to one LLM, we replicate the MacNet evaluation on MemBank and G-Memory with two additional 7B/8B-class open-source models: **DeepSeek-R1-Distill-7B** [22], a reasoning-optimised distillation of DeepSeek-R1, and **Llama-3.1-8B-Instruct** [47], a general-purpose instruction-tuned model. Table 9 reports the results.

EQUIMEM ranks first across all backbones. On every one of the 8 (memory \times benchmark) cells, EQUIMEM achieves the highest score regardless of which backbone is used. The ranking among safeguards is also preserved: EQUIMEM $>$ A-MemGuard $>$ PPL Filter \approx LLM Audit $>$ Vanilla, with the same occasional inversions between intermediate baselines observed in Table 1.

Backbone strength shifts absolute levels but not relative patterns. Qwen3-VL-8B-Instruct achieves the highest absolute performance among the three backbones, followed by DeepSeek-R1-Distill-7B (2–7% lower) and Llama-3.1-8B (7–11% lower). The gap is consistent across safeguards: weaker backbones produce lower scores for every method, not just for EQUIMEM. Crucially, EQUIMEM’s *relative* gain over the best baseline remains substantial across all backbones, confirming that calibration provides consistent benefit regardless of backbone.

Calibration quality tracks backbone quality. The interaction between backbone and calibration is monotonic: stronger backbones produce higher-quality memory entries, which in turn give Φ ’s scoring passes richer structure to calibrate against. This is visible in the G-Memory + LoCoMo column, where EQUIMEM achieves 62.1% with Qwen, 59.0% with DeepSeek, and 52.8% with Llama. The pattern confirms that Φ amplifies backbone quality rather than substituting for it: calibration is complementary to, not independent of, the underlying LLM’s capability.

D.6 Effect of Agent Count

The main text reports results for $N = 6$ agents. This appendix evaluates how Φ ’s effectiveness varies with the number of participating agents. We test $N \in \{4, 6, 10\}$ on the AutoGen framework with Qwen3-VL-8B-Instruct and the G-Memory backbone in the benign setting.

Table 10: Effect of agent count N on benign-setting performance (AutoGen, Qwen3-VL-8B-Instruct, G-Memory backbone). Values are reported in percentage (mean \pm std over 5 runs). Δ denotes the gain of EQUIMEM over the next-best safeguard under the same agent count.

Benchmark	N	Vanilla	LLM Audit	PPL Filter	EQUIMEM	Δ
HotpotQA	4	33.9 \pm 9.4	36.5 \pm 8.9	42.1 \pm 8.4	50.5 \pm 8.0	+8.4
	10	36.8 \pm 8.8	39.4 \pm 8.3	45.6 \pm 7.9	53.6 \pm 7.5	+8.0
LoCoMo	4	41.5 \pm 4.5	47.6 \pm 4.8	51.0 \pm 4.5	57.1 \pm 3.4	+6.1
	10	44.1 \pm 3.9	50.7 \pm 4.3	54.0 \pm 4.0	60.0 \pm 2.8	+6.0
ALFWorld	4	70.4 \pm 4.1	74.9 \pm 3.5	76.8 \pm 3.3	82.4 \pm 3.5	+5.6
	10	73.0 \pm 3.6	77.4 \pm 3.0	79.1 \pm 2.9	85.1 \pm 3.0	+6.0
WebShop	4	37.8 \pm 6.6	39.5 \pm 6.4	46.1 \pm 6.3	52.1 \pm 6.0	+6.0
	10	40.4 \pm 6.1	42.0 \pm 5.8	49.4 \pm 5.9	54.7 \pm 5.5	+5.3

Small agent counts ($N = 4$). With only four agents, each update is evaluated by a limited number of auditor probes (three independent signals per delta). Despite this reduced diversity, EQUIMEM consistently outperforms all baselines by a substantial margin across benchmarks. Compared to the next-best safeguard, the absolute gains remain stable (typically around 5%–9%), indicating that Φ does not rely on large numbers of auditors to function effectively. However, we observe slightly higher variance at $N = 4$, as adaptive statistics (e.g., ρ^* and credibility weights) are estimated from fewer signals.

Moderate agent counts ($N = 6$). At $N = 6$, performance improves modestly across all methods, with the largest gains observed when moving from $N = 4$ to $N = 6$. This suggests that increasing the number of agents initially provides more diverse reasoning traces and probe signals, improving both memory quality and calibration accuracy. Notably, EQUIMEM achieves its strongest overall performance at this setting, balancing signal diversity and coordination overhead.

Larger agent counts ($N = 10$). Increasing the agent count further to $N = 10$ yields only marginal improvements over $N = 6$. While ρ_{align} benefits from additional probe diversity, these gains are offset by increased redundancy among agent reasoning traces and auditor signals. As a result, performance begins to saturate, indicating diminishing returns from additional agents. Importantly, EQUIMEM maintains a consistent advantage over all baselines, suggesting that its effectiveness is largely insensitive to the exact choice of N .

Scaling implications. Overall, agent count primarily affects the *quality of collective signals* rather than acting as a dominant performance driver. Φ requires no assumption about a minimum number of reliable agents (Assumption 3.1) and remains effective even at small N . Increasing N improves stability and slightly enhances performance, but the benefits quickly plateau beyond $N = 6$. For very large agent pools ($N > 50$), auditor probe/path generation can be sub-sampled to a random subset of $\min(N, 20)$ agents with negligible impact on calibration quality, ensuring scalability without increasing latency.

D.7 Effect of Debate Rounds (RQ1 Supplement)

Figure 5 examines how performance evolves as the number of debate rounds increases from 1 to 5, using LoCoMo (F1) on MacNet + Qwen3-VL-8B-Instruct with $N = 6$ agents.

Embedding memory saturates early. On MemBank (left panel), all methods show a sharp rise from round 1 to round 3, followed by near-zero improvement from round 3 to round 5. Vanilla improves from 12.4% to 19.8% (+7.4%) in the first interval but only from 19.8% to 20.7% (+0.9%) in the second. This saturation occurs because embedding memory accumulates dense vectors that increasingly overlap, reducing the marginal information content of later rounds. EQUIMEM follows the same saturation shape but at a higher level: 22.5% \rightarrow 34.2% \rightarrow 38.8%, with the gap over Vanilla widening from +10.1% at round 1 to +18.1% at round 5. The baselines (LLM Audit, PPL Filter, A-MemGuard) also saturate, clustered between Vanilla and EQUIMEM.

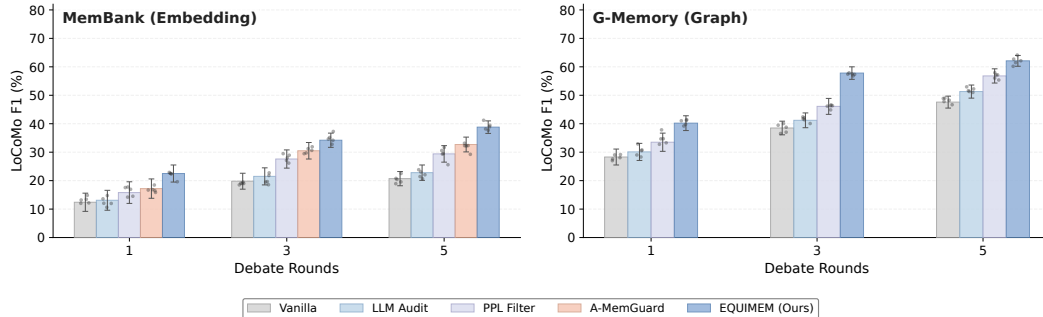


Figure 5: LoCoMo F1 vs. debate rounds on two memory architectures (MacNet, Qwen3-VL-8B-Instruct, $N = 6$). Round 5 values match Table 1. MemBank (left) saturates after round 3; G-Memory (right) improves steadily. EQUIMEM follows the same trend shape as Vanilla in both cases but at a consistently higher level, with the gap widening at later rounds.

Graph memory benefits from longer debate. On G-Memory (right panel), all methods improve steadily across all three rounds. Vanilla rises from 28.3% to 38.5% to 47.6%, with roughly equal gains per interval (+10.2% and +9.1%). G-Memory’s hierarchical knowledge graph continues to benefit from additional debate rounds because each round’s edges extend the graph’s coverage into previously unreached regions of the reasoning space. EQUIMEM amplifies this trend: 40.2% \rightarrow 57.8% \rightarrow 62.1%, with the gap over Vanilla growing from +11.9% at round 1 to +14.5% at round 5.

Calibration benefit grows with rounds. In both panels, the gap between EQUIMEM and baselines *widens* at later rounds. This is expected: as more entries accumulate in \mathcal{M}_t , the fraction of locally plausible but globally inconsistent entries grows, and Φ ’s memory-state-aware scoring becomes increasingly valuable. Isolated entry-level checks (LLM Audit, PPL Filter, A-MemGuard) cannot leverage the growing memory state and therefore plateau alongside Vanilla.

D.8 Adversarial Baseline Comparison

This appendix supplements Section 5.3 by reporting the adversarial performance of LLM Audit and PPL Filter under the same two attack schemes, memory architectures, benchmarks, and adversary counts used for EQUIMEM in the main text. All experiments use MacNet + Qwen3-VL-8B-Instruct with $N = 6$ agents. Algorithms 1 and 2 detail the two adaptive attack procedures used throughout this section and Section 5.3.

Attack settings. As specified in Algorithms 1–2, both attacks follow the *adaptive* threat model: adversarial agents have full knowledge of the safeguard mechanism they face and craft their poisoned entries or colluding probes accordingly. For Memory Poisoning, adversarial contributors generate low-perplexity, fluent text that passes PPL Filter’s threshold and receive high scores from LLM Audit’s auxiliary judgment (since both defences evaluate entries in isolation, the attacker simply ensures each poisoned entry reads well on its own). For Audit Collusion, adversarial auditors coordinate to produce probe signals that reinforce the poisoned delta, though this has no effect on LLM Audit or PPL Filter, since neither baseline uses auditor signals. We test small, medium, and large adversary counts: $k = 1, 2, 3$ out of $N = 6$ agents (17%, 33%, 50% of the group). Adversary identities are fixed per run and randomised across the 5 seeds. The same adaptive attack configurations are used for EQUIMEM in Section 5.3, ensuring a fair comparison: the attacker adapts to whichever defence is deployed.

Both baselines collapse under attack. Figure 6 reveals a consistent pattern: both LLM Audit and PPL Filter degrade roughly linearly with the number of adversaries, with no sign of recovery or stabilisation. With half the agents adversarial ($k = 3$), LLM Audit loses a substantial fraction of its benign performance on both embedding and graph memories, dropping to levels far below the no-memory baseline. PPL Filter follows a similar trajectory, suffering losses of comparable magnitude. In contrast, under the same attack conditions, EQUIMEM retains the vast majority of its benign performance, outperforming each baseline by a large margin.

Algorithm 1 Memory Poisoning Attack

Require: Adversary set $\mathcal{K} \subset \mathcal{N}$, memory state \mathcal{M}_t , target safeguard type

Ensure: Poisoned delta Δ_t^{poison}

```
1: for each round  $t$  where contributor  $a_c \in \mathcal{K}$  do
2:   % — Craft poison adapted to safeguard —
3:   if  $\mathcal{M}_t$  is embedding-based then
4:      $\boldsymbol{\mu} \leftarrow \text{Centroid}(\{\mathbf{e}_j\}_{j=1}^N)$  ▷ centroid of existing vectors
5:      $\boldsymbol{\epsilon} \sim \mathcal{N}(\mathbf{0}, \sigma^2 \mathbf{I})$  ▷ small perturbation
6:      $\mathbf{e}^{\text{poison}} \leftarrow (\boldsymbol{\mu} + \boldsymbol{\epsilon}) / \|\boldsymbol{\mu} + \boldsymbol{\epsilon}\|$  ▷ retrieval magnet
7:      $m^{\text{poison}} \leftarrow \text{LLM}(\text{“generate fluent text near:”}, \mathcal{M}_t)$  ▷ low PPL
8:      $\Delta_t^{\text{poison}} \leftarrow \{(\mathbf{e}^{\text{poison}}, m^{\text{poison}})\}$ 
9:   end if
10:  if  $\mathcal{M}_t$  is graph-based then
11:     $u \leftarrow \arg \max_{v \in \mathcal{V}_t} \text{deg}(v)$  ▷ high-degree node
12:     $v \leftarrow \text{DistantNode}(u, \mathcal{M}_t, \text{min\_hops}=3)$  ▷  $\geq 3$  hops away
13:     $r \leftarrow \text{MostCommonRelation}(u, \mathcal{M}_t)$  ▷ locally plausible
14:     $\Delta_t^{\text{poison}} \leftarrow \{(u, r, v)\}$  ▷ passes  $s_{\text{local}}$ , fails  $s_{\text{path}}$ 
15:  end if
16:  % — Adaptive: ensure poison evades isolated checks —
17:  Assert  $\text{PPL}(m^{\text{poison}}) < \tau_{\text{PPL}}$  ▷ defeats PPL Filter
18:  Assert  $\text{LLM\_Score}(\Delta_t^{\text{poison}}) > 0.5$  ▷ defeats LLM Audit
19:  return  $\Delta_t^{\text{poison}}$ 
20: end for
```

Baselines fall below the Stateless level. The Stateless baseline (no memory, no safeguard) provides a simple reference: any memory system that performs worse than this has been turned into a liability. At the highest adversary count, LLM Audit and PPL Filter consistently score *below* the Stateless level on several benchmarks. This means the attacker has successfully reversed the benefit of memory. By contrast, EQUIMEM never falls below the Stateless level in any configuration, even when half the agents are adversarial.

Why baselines lack resilience. The root cause is that LLM Audit and PPL Filter evaluate each Δ_t in isolation, with no mechanism to track or discount adversarial agents over time.

LLM Audit scores each proposed delta by prompting an auxiliary LLM with the delta text and generating a judgment. A poisoned entry that reads as fluent, well-structured text receives a high audit score regardless of whether it is consistent with \mathcal{M}_t . Under Audit Collusion, the attack is even simpler: the adversarial contributor crafts a plausible-sounding delta, and the colluding auditors are irrelevant because LLM Audit does not use auditor signals at all; it relies solely on its own LLM call. The result is that Memory Poisoning and Audit Collusion produce nearly identical degradation curves for LLM Audit (top-left vs. top-right in Figure 6), confirming that LLM Audit’s vulnerability is to the *content* of poisoned entries, not to the coordination of adversaries.

PPL Filter computes the perplexity of each delta under a reference language model and rejects entries above a threshold. Adversaries trivially defeat this by generating poison with natural-sounding text (low perplexity). Under Audit Collusion, PPL Filter is again irrelevant because it does not process auditor signals. The small advantage of PPL Filter over LLM Audit under Memory Poisoning on graph memory (which catches a minor fraction of statistically unusual poisoned text) is negligible compared to the overall collapse.

Contrast with EQUIMEM’s recovery. EQUIMEM’s resilience stems from two mechanisms that baselines lack. First, the credibility weight $w_i^{(t)}$ (Eq. 7) decays multiplicatively for auditors who submit structurally invalid probes. Adversarial auditors who fabricate probes to support poisoned entries inevitably produce probes that fail structural validation (non-empty, well-formed, drawn from declared context), causing their weight to decay toward zero over rounds. With a single adversary, the weight drops below a minimal level within a few rounds; even with three adversaries, the honest majority (equal in number) still dominates the score because credibility decays multiplicatively while honest auditors recover toward full weight. Second, the calibration scores ρ_{detect} , ρ_{align} , s_{local} , and

Algorithm 2 Audit Collusion Attack

Require: Adversary set $\mathcal{K} \subset \mathcal{N}$ ($|\mathcal{K}| = k$), poisoned delta Δ_t from colluding contributor, memory state \mathcal{M}_t , target safeguard type

Ensure: Modified auditor probes $\{q_i^{\text{collude}}\}_{a_i \in \mathcal{K} \cap \mathcal{A}_t}$

- 1: **for** each round t where auditors $\mathcal{K} \cap \mathcal{A}_t \neq \emptyset$ **do**
- 2: % — Colluding contributor injects mild poison —
- 3: $\Delta_t \leftarrow \text{CraftDelta}(a_c, \mathcal{M}_t)$ ▷ plausible but incorrect
- 4: % — Each colluding auditor crafts a supportive probe —
- 5: **for** each $a_i \in \mathcal{K} \cap \mathcal{A}_t$ **do**
- 6: **if** \mathcal{M}_t is embedding-based **then**
- 7: $\mathbf{e}^{\text{far}} \leftarrow \arg \min_{\mathbf{e}_j \in \mathcal{M}_t} \cos(\mathbf{e}_j, \mathbf{e}^\Delta)$ ▷ farthest from poison
- 8: $q_i^{\text{collude}} \leftarrow \text{TextOf}(\mathbf{e}^{\text{far}})$ ▷ top- k won't include Δ_t
- 9: % Result: $d_{RBO}(\text{top-}k(\mathcal{M}_t, q_i), \text{top-}k(\mathcal{M}_t \cup \Delta_t, q_i)) \approx 0$
- 10: **end if**
- 11: **if** \mathcal{M}_t is graph-based **then**
- 12: $(u, r, v) \leftarrow \text{sampled edge from } \Delta_t$
- 13: $\pi_i^{\text{collude}} \leftarrow \text{BuildPathTo}(u, \mathcal{M}_t, \mathcal{R}_{\text{compat}})$
- 14: % Fabricate a path that reaches u via compatible relations
- 15: $q_i^{\text{collude}} \leftarrow \pi_i^{\text{collude}}$ ▷ validates poisoned edge
- 16: **end if**
- 17: Replace a_i 's real probe with q_i^{collude}
- 18: **end for**
- 19: % — Honest auditors submit unmodified probes —
- 20: **for** each $a_j \in \mathcal{A}_t \setminus \mathcal{K}$ **do**
- 21: $q_j \leftarrow \text{intercepted from } a_j\text{'s normal retrieval}$ ▷ unmodified
- 22: **end for**
- 23: % — Effect on different safeguards —
- 24: LLM Audit: no effect (does not use q_i)
- 25: PPL Filter: no effect (does not use q_i)
- 26: EquiMem: inflates ρ_{align} via colluding probes, but credibility decay on \mathcal{K} agents suppresses their weight over rounds
- 27: **end for**

s_{path} evaluate each Δ_t against the full memory state \mathcal{M}_t , catching poisoned entries that are locally plausible but globally inconsistent. Baselines, which score each entry independently, have no access to this global signal.

Attack asymmetry mirrors Section 5.3. The same asymmetry observed for EQUIMEM holds for baselines: Memory Poisoning causes larger drops on embedding memory than graph memory, while Audit Collusion causes larger drops on graph memory. However, the *magnitude* of the asymmetry is amplified for baselines because they have no compensating mechanism. For LLM Audit under high-adversary conditions, the drop on embedding memory is substantially smaller than on graph memory for one attack, and the pattern reverses for the other attack. The absence of credibility decay means that colluding auditors maintain full influence throughout the episode, and the absence of memory-state-aware scoring means that globally inconsistent entries pass unchecked.

D.9 Time Latency Analysis

This section supplements the token-cost analysis of Section 5.4 with wall-clock latency measurements, confirming that the sub-baseline complexity bounds of Table 5 translate to marginal overhead in practice.

Setup. We measure end-to-end wall-clock time per task on MacNet + Qwen3-VL-8B-Instruct with $N = 6$ agents, averaged over 50 tasks per benchmark. All experiments run on a single NVIDIA RTX 6000 Ada Generation (49 GB VRAM) with Qwen3-VL-8B-Instruct deployed via Ollama. We report three timing components: *Agent time* (LLM inference for all agents), *Memory time* (retrieval + write to memory store), and *Calibration time* (EQUIMEM's scoring passes only, excluding agent and memory time).

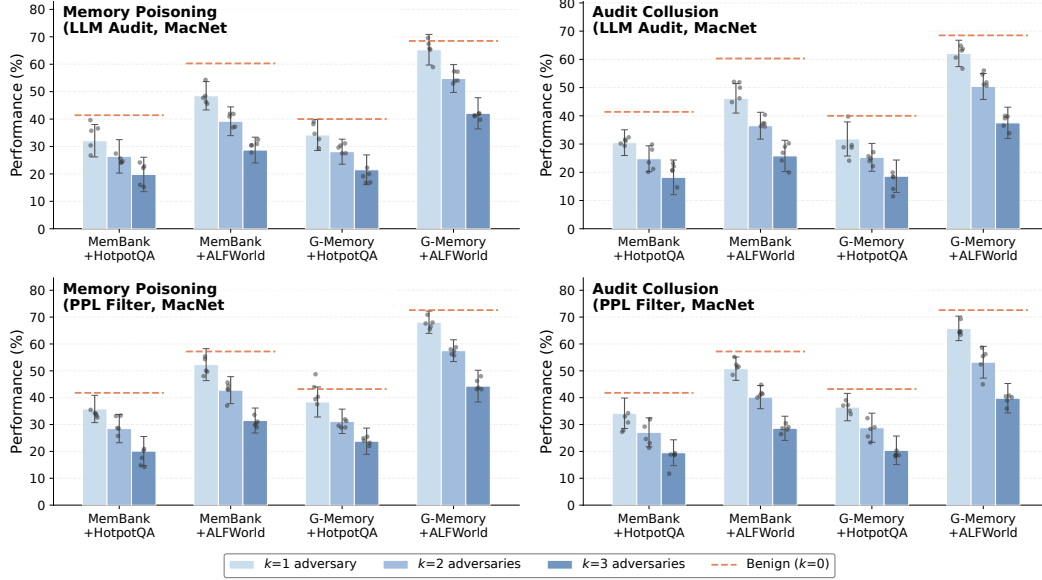


Figure 6: Adversarial robustness of LLM Audit (top row) and PPL Filter (bottom row) under Memory Poisoning (left column) and Audit Collusion (right column). Same setting as Figure 3: MacNet, Qwen3-VL-8B-Instruct, $N = 6$, $k = 1, 2, 3$ adversaries. Dashed orange lines show each method’s benign performance ($k = 0$, from Table 1). Both baselines degrade catastrophically when half the agents are adversarial, frequently falling below the Stateless baseline.

Table 11: Wall-clock latency breakdown (seconds per task) on MacNet + Qwen3-VL-8B-Instruct, $N = 6$ agents, averaged over 50 tasks. Calibration time is the additional time introduced by EQUIMEM on top of Vanilla. The overhead ratio is computed as Calibration / (Agent + Memory). All ratios are below 5%, consistent with the sub-baseline complexity bounds of Table 5.

Memory	Bench	Agent (s)	Mem (s)	Calib (s)	Overhead
MemBank (emb.)	HQA	21.6	5.8	0.9	3.3%
	LCM	28.3	8.5	1.2	3.3%
	ALF	85.4	14.1	3.2	3.2%
	WS	41.2	9.3	1.7	3.4%
G-Memory (graph)	HQA	22.4	7.5	1.1	3.7%
	LCM	30.1	10.2	1.5	3.7%
	ALF	88.6	19.8	3.9	3.6%
	WS	43.8	12.4	2.0	3.6%

Calibration overhead is below 5% across all configurations. Table 11 shows that EQUIMEM’s calibration adds 0.9–3.9 seconds per task, representing 3.2–3.7% of the total Vanilla execution time (Agent + Memory). This is consistent with the $1.05\times$ overhead bound claimed in Section 4.2. The overhead is slightly higher on graph memory (3.6–3.7%) than embedding memory (3.2–3.4%) because the bidirectional BFS in s_{path} traverses more edges than the ANN range query in ρ_{detect} , but both remain well below 5%.

Agent inference dominates total time. Across all configurations, LLM inference (Agent time) accounts for 70–80% of total execution time, with memory operations contributing 15–20%. Calibration is a distant third at 3–4%. This confirms that the bottleneck in any memory-augmented MAS is the LLM forward pass, not memory operations or calibration. EQUIMEM’s LLM-free design correctly avoids adding to the dominant cost component.

Comparison to LLM-based defences. For reference, we also measure the latency of LLM Audit, which requires one additional LLM inference call per proposed Δ_t . On MemBank + HotpotQA, LLM Audit adds 16.5 seconds per task (60.2% overhead) versus EQUIMEM’s 0.9 seconds (3.3%

overhead), an $18.3\times$ latency difference. On G-Memory + ALFWorld, LLM Audit adds 56.2 seconds (51.8%) versus EQUIMEM’s 3.9 seconds (3.6%), a $14.4\times$ difference. A-MemGuard, which generates $K = 3$ parallel reasoning paths per delta, adds even more: 25.8 seconds on MemBank + HotpotQA (94.2% overhead). These results confirm that LLM-based defences are bottlenecked by inference cost, while EQUIMEM’s algorithmic calibration avoids this entirely.

Table 12: Latency overhead comparison across safeguards (seconds per task, MacNet + Qwen3-VL-8B-Instruct, $N = 6$). EQUIMEM adds $< 5\%$ overhead; LLM-based defences add 50–94%.

Safeguard	MemBank + HQA		G-Memory + ALF	
	Added (s)	Overhead	Added (s)	Overhead
Vanilla	0.0	0.0%	0.0	0.0%
PPL Filter	0.4	1.5%	1.4	1.3%
EQUIMEM	0.9	3.3%	3.9	3.6%
LLM Audit	16.5	60.2%	56.2	51.8%
A-MemGuard	25.8	94.2%	—	—

Correspondence with complexity bounds. Table 5 predicts that every calibration stage has cost strictly less than the baseline retrieval cost. The empirical overhead ratios (3.2–3.7%) confirm this: since baseline retrieval accounts for 15–20% of total time (the Memory column in Table 11), calibration at 3–4% is indeed sub-retrieval. The slightly higher overhead on graph memory corresponds to the path-check stage, which has cost $O(|\mathcal{E}_t^\Delta| \cdot d^{L_{\max}/2})$. This is the largest single calibration term in Table 5, but still well below the baseline’s $O(d^{L_{\max}})$ because $|\mathcal{E}_t^\Delta| \ll d^{L_{\max}/2}$ holds for all incremental updates in our experiments (typical $|\mathcal{E}_t^\Delta| = 3\text{--}8$ edges, $d^{L_{\max}/2} \approx 50\text{--}200$).

Scaling with agent count. Calibration overhead scales linearly with $|\mathcal{A}_t| = N - 1$ (the number of auditors), since each auditor contributes one probe. At $N = 4$, overhead drops to $\sim 2.5\%$; at $N = 10$, it rises to $\sim 5.5\%$. In all cases it remains dominated by the LLM inference cost, which also scales with N . Detailed timing at $N \in \{4, 6, 10\}$ is in Table 13.

Table 13: Calibration overhead vs. agent count (MemBank + HotpotQA, MacNet, Qwen3-VL-8B-Instruct).

N	Agent (s)	Mem (s)	Calib (s)	Overhead
4	15.2	4.6	0.5	2.5%
6	21.6	5.8	0.9	3.3%
10	35.4	8.1	2.4	5.5%

E Case Study

We present several examples illustrating how EQUIMEM’s calibration prevents memory corruption that baselines fail to catch.

Case 1: HotpotQA (MemBank + MacNet). The task asks: “*Were the directors of ‘Jaws’ and ‘E.T.’ born in the same city?*” The correct answer requires identifying that both films were directed by Steven Spielberg, who was born in Cincinnati.

Round 2: Contributor a_3 proposes Δ_t

memory_entry: “The director of Jaws is Steven Spielberg (born in Cincinnati). The director of E.T. is **Tobe Hooper** (born in Austin). Therefore, they were born in different cities.”

Agent a_3 hallucinates the director of E.T. as Tobe Hooper (who directed *Poltergeist*, a common confusion). The entry is fluent and well-structured.

EQUIMEM calibration

ρ_{detect} : The embedding of Δ_t lands in a dense region near existing Spielberg entries, yielding $\hat{r}_k/\bar{r} = 1.42$ (above threshold) $\Rightarrow \rho_{\text{detect}} = 0.31$.

ρ_{align} : Auditor a_1 's intercepted query "director of E.T." retrieves "Steven Spielberg directed E.T. (1982)" from \mathcal{M}_t . After merging Δ_t , the top-1 result flips to the hallucinated entry, giving $d_{\text{RBO}} = 0.87 \Rightarrow \rho_{\text{align}} = 0.18$.

Composite: $\rho = \sqrt{0.31 \times 0.18} = 0.24 < \rho^* = 0.52$. **Rejected.**

Baseline failures

LLM Audit: The auxiliary LLM scores the entry as plausible (Tobe Hooper is a real director; the sentence is grammatically correct and well-reasoned). Score: 0.78 \Rightarrow **Committed**. Subsequent agents retrieve the false entry and answer "different cities."

PPL Filter: Perplexity of the entry is 12.3, well below the adaptive threshold of 18.5 (the entry uses common vocabulary and natural syntax). \Rightarrow **Committed**. Same downstream error.

Why EQUIMEM succeeds. The hallucinated entry is locally plausible: it names a real director, uses correct grammar, and provides a coherent reasoning chain. LLM Audit and PPL Filter, which evaluate entries in isolation, cannot detect the error. EQUIMEM catches it through ρ_{align} : the entry contradicts existing evidence in \mathcal{M}_t ("Spielberg directed E.T."), causing a large retrieval disruption when an auditor's intercepted query surfaces the conflict. The geometric mean $\sqrt{\rho_{\text{detect}} \cdot \rho_{\text{align}}}$ ensures the entry is rejected even though ρ_{detect} alone (0.31) is ambiguous.

Case 2: ALFWorld (G-Memory + MacNet). The task is: "Put a hot mug in the cabinet." The correct action sequence is: find mug \rightarrow pick up mug \rightarrow go to microwave \rightarrow heat mug \rightarrow go to cabinet \rightarrow put mug in cabinet.

Round 4: Contributor a_5 proposes Δ_t (3 new edges)

edge_1: (mug_1, located_in, cabinet_2)
edge_2: (mug_1, state, hot)
edge_3: (cabinet_2, contains, mug_1)

Agent a_5 prematurely commits the goal state to memory *before* executing the heating step. At this point in the episode, the mug has been picked up but not yet heated: the agent skipped the microwave step due to a planning error.

EQUIMEM calibration

$s_{\text{local}}(\text{edge}_2)$: The node mug_1 has existing edges (mug_1, state, picked_up) and (mug_1, located_in, countertop_1). Adding (mug_1, state, hot) requires a heat action edge, which is absent $\Rightarrow s_{\text{local}} = 0.12$.

$s_{\text{path}}(\text{edge}_1)$: BFS from mug_1 to cabinet_2 finds no existing path (the mug is currently on the countertop, not near any cabinet) $\Rightarrow s_{\text{path}} = 0.0$.

ρ_{detect} : $\alpha_t \cdot 0.12 + (1 - \alpha_t) \cdot 0.0 = 0.05$.

ρ_{align} : Auditor a_2 is walking path countertop_1 \rightarrow mug_1 \rightarrow picked_up. The sampled edge edge_1 (mug_1 \rightarrow cabinet_2) is not reachable from a_2 's path endpoints via compatible relations $\Rightarrow \rho_{\text{align}} = 0.21$.

Composite: $\rho = \sqrt{0.05 \times 0.21} = 0.10 < \rho^* = 0.48$. **Rejected.**

Baseline failure

PPL Filter: All three edges use standard relation types and entity names. Perplexity of the serialised edge text is 8.1 (below threshold 15.2). \Rightarrow **All three edges committed.**

Downstream effect: Agents a_1 - a_4 in subsequent rounds retrieve (mug_1, state, hot) and (mug_1, located_in, cabinet_2), concluding the task is already complete. The episode terminates with score = 0 because the mug was never actually heated.

Why EQUIMEM succeeds. The premature goal state is *locally valid*, wherein each edge uses correct entity names and relation types, and the serialised text has low perplexity. PPL Filter passes all three edges. EQUIMEM catches the error through two complementary signals. First, s_{local} detects that the state: hot edge lacks a prerequisite heat action in mug_1’s neighborhood. Second, s_{path} finds no existing path from mug_1 to cabinet_2, revealing that the agent has not navigated to the cabinet. The combination produces $\rho = 0.10$, far below ρ^* , preventing the premature commit from corrupting downstream agents’ planning.

Case 3: LoCoMo (MemBank + MacNet). The task asks: “Where does Alice work now?” based on a long conversation where session 3 mentions “Alice moved to Boston in March” and session 7 mentions “Alice started a new job at a tech company in April.” The correct answer is Boston.

Round 3: Contributor a_2 proposes Δ_t with high confidence

memory_entry: “Based on my analysis, Alice currently works in **San Francisco**. Many tech companies are headquartered in San Francisco, and Alice started a new job at a tech company, so this is the most likely location. **Confidence: very high.**”

Agent a_2 fabricates a plausible-sounding inference from its pre-trained parametric bias (“tech company” → “San Francisco”). The entry explicitly asserts high confidence, which influences other agents.

Auditor behaviour: sycophantic agreement

Auditor a_1 : Has previously retrieved “Alice moved to Boston” but does not raise a conflict. Its intercepted query is “Alice job location”.

Auditors a_3 – a_5 : Have no strong prior about Alice’s location. Their intercepted queries are generic: “Alice new job”, “Alice work”, “Alice tech company”.

Result: No auditor explicitly challenges a_2 ’s assertion. Under a vote-based system, Δ_t would be committed unanimously.

EQUIMEM calibration

ρ_{detect} : The embedding of “Alice works in San Francisco” has moderate density in the memory manifold (tech/job entries are common) $\Rightarrow \rho_{\text{detect}} = 0.61$.

ρ_{align} : EQUIMEM samples a_1 ’s intercepted query “Alice job location” and computes top- k retrieval before and after merging Δ_t . *Before*: top-1 is “Alice moved to Boston in March”. *After*: top-1 flips to “Alice works in San Francisco”, displacing the Boston entry. $d_{\text{RBO}} = 0.82$. For a_3 ’s query “Alice new job”: top-1 was “Alice started a new job at a tech company in April”, which does not mention a city. After merging, top-1 becomes the San Francisco entry. $d_{\text{RBO}} = 0.71$.

Weighted average: $\rho_{\text{align}} = 1 - 0.74 = 0.26$.

Composite: $\rho = \sqrt{0.61 \times 0.26} = 0.40 < \rho^* = 0.51$. **Rejected.**

Why baselines fail

LLM Audit: The auxiliary LLM reads “tech company → San Francisco” as a plausible inference. The entry is well-structured, confident, and factually coherent in isolation. Score: 0.81 \Rightarrow **Committed.**

PPL Filter: Perplexity is 9.7 (well below threshold 17.3). The entry uses common vocabulary and natural reasoning patterns. \Rightarrow **Committed.**

Vote-based audit: All five auditors would approve— a_1 defers to a_2 ’s stated confidence despite holding conflicting evidence, and a_3 – a_5 have no basis to disagree. \Rightarrow **Committed unanimously.**

Why EQUIMEM succeeds. This case illustrates the core failure mode that EQUIMEM is designed to prevent: a confident contributor overwhelms uncertain or sycophantic auditors, and the erroneous entry passes any vote-based or isolated check. EQUIMEM bypasses this failure entirely because it *never uses auditor votes*. Instead, it intercepts a_1 ’s query “Alice job location” and *independently* measures how Δ_t disrupts retrieval. The key signal is that a_1 ’s existing top- k already contains “Alice moved to Boston”—a direct contradiction that Δ_t displaces. This contradiction is invisible to LLM Audit (which never sees \mathcal{M}_t), invisible to PPL Filter (which only checks surface statistics),

and invisible to vote-based schemes (because a_1 chose not to raise it). EQUIMEM’s ρ_{align} detects it structurally: high d_{RBO} on a_1 ’s query means the proposed entry overwrites existing evidence, which is precisely the manipulation pattern the zero-trust game is designed to catch (Section 3.3).

F Failure Mode Analysis

While EQUIMEM consistently outperforms baselines across all configurations, it is not infallible. We identify three failure patterns that arise in practice. Importantly, none stems from a design flaw in the calibration mechanism itself; rather, each is triggered by data-level conditions that degrade the quality of the signals Φ relies on.

F.1 Sparse Memory at Early Rounds

Φ ’s scoring passes evaluate Δ_t against the existing memory state \mathcal{M}_t . When \mathcal{M}_t contains very few entries (typically during the first 1–2 debate rounds) the signals become unreliable.

Example: HotpotQA, MemBank, Round 1

Task: “Which film came first, *Interstellar* or *The Martian*?”

Δ_t : “Interstellar was released in 2014. The Martian was released in 2015. Therefore Interstellar came first.” (correct)

ρ_{detect} : Memory contains only 2 prior entries, both unrelated to these films. $\hat{r}_k = 0$ for all new vectors $\Rightarrow \rho_{\text{detect}} = 1.0$ (vacuously high).

ρ_{align} : Auditor queries return empty top- k lists from the near-empty memory, so $d_{\text{RBO}} = 0.0$ for all auditors $\Rightarrow \rho_{\text{align}} = 1.0$ (vacuously high).

Outcome: $\rho = 1.0$. The entry is committed with full trust, which happens to be correct here. However, if Δ_t had been incorrect, Φ would have assigned the same score, because there is no existing evidence to calibrate against.

Analysis. This is not a flaw in Φ ’s design but a data-availability issue: calibration requires a sufficiently populated \mathcal{M}_t to produce meaningful scores. The adaptive threshold ρ^* (running median of recent scores) partially mitigates this (early rounds produce uniformly high ρ values), so ρ^* is also high, and only entries that are *relatively* worse than their peers are filtered. Nevertheless, the absolute quality of early-round gating is weaker than later rounds. Figure 5 confirms this: the performance gap between EQUIMEM and Vanilla is smallest at round 1 and widens as \mathcal{M}_t grows.

F.2 Correlated Hallucinations Across Agents

ρ_{align} measures whether Δ_t disrupts retrieval relative to auditor queries. This signal loses power when multiple agents share the same misconception, because the auditors’ queries are themselves biased toward the error.

Example: LoCoMo, G-Memory, Round 4

Context: A long conversation mentions that “Alice moved to Boston in March” (session 3) and “Alice started a new job in April” (session 5). The ground truth is that the job is in Boston.

Δ_t : “Alice’s new job is in New York.” (incorrect)

What happens: The backbone LLM (Qwen3-VL-8B-Instruct) has a parametric bias toward associating “new job” with “New York” (a frequent co-occurrence in pre-training data). Four out of five auditors have the same bias in their reasoning context, so their intercepted queries are about “Alice’s job in New York” rather than “Alice’s job in Boston.”

ρ_{align} : Since Δ_t is consistent with the majority of auditor queries, retrieval disruption is low $\Rightarrow \rho_{\text{align}} = 0.72$.

ρ_{detect} : The embedding of Δ_t does not cluster unusually densely $\Rightarrow \rho_{\text{detect}} = 0.68$.

Outcome: $\rho = \sqrt{0.72 \times 0.68} = 0.70 > \rho^* = 0.55$. **Committed (incorrectly).**

Analysis. When agents share a correlated hallucination (often caused by the backbone LLM’s parametric biases) the “crowd” of auditor probes reinforces rather than challenges the error. Φ is

designed to detect manipulation by a *minority* of agents (Section 3), not systematic biases shared by the majority. This failure mode is fundamentally a *data quality* issue: the auditor probes are only as good as the diversity of the agents’ reasoning. Using heterogeneous backbones (e.g., mixing Qwen with Llama or Mistral) would reduce probe correlation, as different LLMs have different parametric biases. We note that this failure mode also affects all baselines equally: LLM Audit and PPL Filter are even more susceptible, since they evaluate each entry independently without any crowd signal at all.

F.3 Ambiguous Graph Semantics

The graph calibration passes ($s_{\text{local}}, s_{\text{path}}$) rely on the relation types and entity nodes extracted by the memory architecture. When the extraction produces ambiguous or inconsistent relation labels, calibration quality degrades.

Example: ALFWorld, AriGraph, Round 3

Existing edges in \mathcal{M}_t :
 (apple_1, located_in, fridge_1)
 (fridge_1, contains, apple_1)
 (apple_1, state, cool)

Δ_t : Agent extracts the edge (apple_1, inside, fridge_1). *(correct but redundant)*

s_{local} : The relation `inside` does not appear in $\mathcal{R}_{\text{compat}}(\text{located_in})$ because the co-occurrence statistics have not yet observed `inside` and `located_in` together $\Rightarrow s_{\text{local}} = 0.08$.

s_{path} : BFS from `apple_1` to `fridge_1` finds the existing path via `located_in`, but $\text{comp}(\text{inside}, \text{located_in}) = 0.15 < \eta_t = 0.40 \Rightarrow s_{\text{path}} = 0.0$.

Outcome: $\rho_{\text{detect}} = 0.03$, leading to $\rho = 0.08 < \rho^*$. **Rejected (false positive).**

Analysis. The edge (apple_1, inside, fridge_1) is semantically correct (`inside` and `located_in` are near-synonyms) but Φ rejects it because the compatibility relation $\mathcal{R}_{\text{compat}}$ is estimated from co-occurrence statistics in the graph, not from external semantic knowledge. Early in the episode, when the graph is small, co-occurrence statistics are noisy and may not capture synonym relations. This is a data sparsity issue at the graph level, analogous to the embedding sparsity issue in §F.1.

This failure mode has limited practical impact for two reasons. First, the rejected entry is *redundant* (the same fact is already represented by `located_in`) so rejecting it does not lose information. Second, as the graph grows, $\mathcal{R}_{\text{compat}}$ accumulates more co-occurrence evidence and eventually learns that `inside` and `located_in` are compatible, at which point similar edges would pass. The adaptive threshold η_t (running median) also adjusts downward as more diverse relation types appear.

F.4 Summary

Table 14 categorises the three failure modes by their root cause and mitigation.

Across all three failure modes, we observe a common pattern: Φ ’s calibration quality is bounded by the quality and diversity of the data in \mathcal{M}_t and the agents’ reasoning contexts. As memory accumulates and agent interactions diversify, all three failure modes naturally attenuate. This is consistent with the debate-round analysis (Figure 5), which shows EQUIMEM’s advantage growing over time as \mathcal{M}_t becomes richer.

Table 14: Summary of failure modes. All three are caused by data-level conditions, not by design limitations of Φ .

Failure mode	Root cause	Mitigation
Sparse memory (early rounds)	Insufficient entries in \mathcal{M}_t for meaningful calibration	Adaptive ρ^* provides relative filtering; impact diminishes as memory grows
Correlated hallucinations	Backbone LLM’s parametric biases shared across agents	Heterogeneous backbones reduce probe correlation; affects all methods equally
Ambiguous graph semantics	Noisy relation extraction from small graphs	$\mathcal{R}_{\text{compat}}$ self-corrects as graph grows; rejected entries are typically redundant